strongly associated with neurodegeneration and cognitive impairment [7, 33]. As shown in Fig. 6, patients with moderate to severe AD tended to show greater neocortical [^{18}F]THK-5117 retention, which corresponds to Braak stages V/VI. The difference in hippocampal uptake of [^{18}F]THK-5117 between HCs and AD patients was not as robust as we had expected. This may have been caused by the elevated [^{18}F]THK-5117 accumulation in the hippocampus of HCs and the underestimation of hippocampal retention due to atrophy in patients with AD. This result is consistent with the post-mortem finding that hippocampal tau deposits are also frequently observed in nondemented elderly people [35–37].

Many PET tracers have recently been proposed for imaging tau in the human brain. [^{18}F]FDDNP was the first PET tracer that successfully visualized tau pathology in the human brain [38, 39]. However, this tracer reportedly binds nonselectively to both Aβ and tau in AD brains [40]. Recently, [^{11}C]PBB3 has been reported as a selective tau tracer [22]. A PET study successfully demonstrated [^{11}C]PBB3 retention in the hippocampus and neocortex of patients with AD and in the basal ganglia of patients with corticobasal degeneration. However, the short radioactive half-life of ^{11}C restricts the use of [^{11}C]PBB3 to a few PET centres. Two ^{18}F-labelled PET tracers, [^{18}F]T807 and [^{18}F]T808, have recently been reported and clinically tested [19–21]. A first-in-human [^{18}F]T807 PET study has demonstrated that the neocortical [^{18}F]T807 retention follows the known distribution of tau pathology in AD brain [20]. In two patients with AD, [^{18}F]T807 retention was reported to be higher in the lateral temporal cortex than in the frontal cortex. These results are similar to our PET findings. Nevertheless, the main advantage of [^{18}F]THK-5117 over [^{18}F]T807 is its better kinetics in the brain. The time taken to reach the plateau of neocortical SUVR values was shorter for [^{18}F]THK-5117 (50 min after injection) than for [^{18}F]T807 (80 min after injection). However, the use of [^{18}F]T807 may allow more accurate visual interpretation of PET images than the use of [^{18}F]THK-5117 because of the former's negligible white matter retention. [^{18}F]THK-5117 retention in the white matter possibly reflects its binding to β-sheet structures contained in myelin, as observed with other amyloid PET tracers [41]. If sufficient tracer signals are observed in the grey matter of the brain, white matter retention will not lead to the misclassification of scans [42]. However, it is important to develop an optimized PET tracer that shows lower nonspecific binding in the white matter than [^{18}F]THK-5117.

[^{18}F]THK-5117 PET demonstrated high tracer retention in sites susceptible to tau deposition in patients with AD. The in vitro selective binding ability of [^{18}F]THK-5117 to tau was confirmed by directly comparing it with the amyloid PET tracer PiB. Although these results should be considered preliminary due to the small sample size, [^{18}F]THK-5117 is a useful PET tracer for the noninvasive evaluation of tau pathology in patients with AD.

Compliance with Ethical Standards

Funding This study was supported by the research fund from GE Healthcare, the SEI (Sumitomo Electric Industries, Ltd.) Group CSR Foundation, the Industrial Technology Research Grant Program of the NEDO in Japan (09E51025a), Health and Labor Sciences Research Grants from the Ministry of Health, Labor, and Welfare of Japan, a Grant-in-Aid for Scientific Research (B) (23390297), a Grant-in-Aid for Scientific Research on Innovative Areas (26117003) and "Japan Advanced Molecular Imaging Program (J-AMP)" of the Ministry of Education, Culture, Sports, Science and Technology (MEXT), Japan.

Conflicts of interest Yukitsuka Kudo, Nobuyuki Okamura and Shozo Furumoto received research grants from GE Healthcare. Yukitsuka Kudo also received research grants from Sumitomo Electric Industries. Yukitsuka Kudo and Nobuyuki Okamura own stock in Clino Ltd.

Ethical approval All procedures performed in studies involving human participants were in accordance with the ethical standards of the institutional and/or national research committee and with the 1964 Helsinki declaration and its later amendments or comparable ethical standards. This article does not contain any studies with animals performed by any of the authors.

Informed consent Informed consent was obtained from all individual participants included in the study.

References

1. Braak H, Braak E. Neuropathological stageing of Alzheimer-related changes. Acta Neuropathol. 1991;82:239–59.
2. Masters CL, Simms G, Weinman NA, Multhaup G, McDonald BL, Beyreuther K. Amyloid plaque core protein in Alzheimer disease and Down syndrome. Proc Natl Acad Sci U S A. 1985;82:4245–9.
3. Grundke-Iqbal I, Iqbal K, Quinlan M, Tung YC, Zaidi MS, Wisniewski HM. Microtubule-associated protein tau. A component of Alzheimer paired helical filaments. J Biol Chem. 1986;261:6084–9.
4. Grundke-Iqbal I, Iqbal K, Tung YC, Quinlan M, Wisniewski HM, Binder LI. Abnormal phosphorylation of the microtubule-associated protein tau (tau) in Alzheimer cytoskeletal pathology. Proc Natl Acad Sci U S A. 1986;83:4913–7.
5. Braak H, Braak E. Frequency of stages of Alzheimer-related lesions in different age categories. Neurobiol Aging. 1997;18:351–7.
6. Bierer LM, Hof PR, Purohit DP, Carlin L, Schmeidler J, Davis KL, et al. Neocortical neurofibrillary tangles correlate with dementia severity in Alzheimer's disease. Arch Neurol. 1995;52:81–8.
7. Gomez-Isla T, Hollister R, West H, Mui S, Growdon JH, Petersen RC, et al. Neuronal loss correlates with but exceeds neurofibrillary tangles in Alzheimer's disease. Ann Neurol. 1997;41:17–24. doi:10.1002/ana.410410106.
8. Arriagada PV, Growdon JH, Hedley-Whyte ET, Hyman BT. Neurofibrillary tangles but not senile plaques parallel duration and severity of Alzheimer's disease. Neurology. 1992;42:631–9.
9. Wilcock GK, Esiri MM. Plaques, tangles and dementia. A quantitative study. J Neurol Sci. 1982;56:343–56.
10. Arnold SE, Hyman BT, Flory J, Damasio AR, Van Hoesen GW. The topographical and neuroanatomical distribution of neurofibrillary tangles and neuritic plaques in the cerebral cortex of patients with Alzheimer's disease. Cereb Cortex. 1991;1:103–16.

11. Gotz J, Ittner A, Ittner LM. Tau-targeted treatment strategies in Alzheimer's disease. Br J Pharmacol. 2012;165:1246–59. doi:10.1111/j.1476-5381.2011.01713.x.
12. Wischik CM, Harrington CR, Storey JM. Tau-aggregation inhibitor therapy for Alzheimer's disease. Biochem Pharmacol. 2014;88:529–39. doi:10.1016/j.bcp.2013.12.008.
13. Citron M. Alzheimer's disease: strategies for disease modification. Nat Rev Drug Discov. 2010;9:387–98. doi:10.1038/nrd2896.
14. Takashima A. Tau aggregation is a therapeutic target for Alzheimer's disease. Curr Alzheimer Res. 2010;7:665–9.
15. Jack Jr CR, Holtzman DM. Biomarker modeling of Alzheimer's disease. Neuron. 2013;80:1347–58. doi:10.1016/j.neuron.2013.12.003.
16. Cummings JL. Biomarkers in Alzheimer's disease drug development. Alzheimers Dement. 2011;7:e13–44. doi:10.1016/j.jalz.2010.06.004.
17. Arai H, Terajima M, Miura M, Higuchi S, Muramatsu T, Machida N, et al. Tau in cerebrospinal fluid: a potential diagnostic marker in Alzheimer's disease. Ann Neurol. 1995;38:649–52. doi:10.1002/ana.410380414.
18. Itoh N, Arai H, Urakami K, Ishiguro K, Ohno H, Hampel H, et al. Large-scale, multicenter study of cerebrospinal fluid tau protein phosphorylated at serine 199 for the antemortem diagnosis of Alzheimer's disease. Ann Neurol. 2001;50:150–6.
19. Xia CF, Arteaga J, Chen G, Gangadharmath U, Gomez LF, Kasi D, et al. [(18)F]T807, a novel tau positron emission tomography imaging agent for Alzheimer's disease. Alzheimers Dement. 2013;9:666–76. doi:10.1016/j.jalz.2012.11.008.
20. Chien DT, Bahri S, Szardenings AK, Walsh JC, Mu F, Su MY, et al. Early clinical PET imaging results with the novel PHF-tau radioligand [F-18]-T807. J Alzheimers Dis. 2013;34:457–68. doi:10.3233/JAD-122059.
21. Chien DT, Szardenings AK, Bahri S, Walsh JC, Mu FR, Xia CF, et al. Early clinical PET imaging results with the novel PHF-Tau radioligand [F18]-T808. J Alzheimers Dis. 2014;38:171–84. doi:10.3233/Jad-130098.
22. Maruyama M, Shimada H, Suhara T, Shinotoh H, Ji B, Maeda J, et al. Imaging of tau pathology in a tauopathy mouse model and in Alzheimer patients compared to normal controls. Neuron. 2013;79:1094–108. doi:10.1016/j.neuron.2013.07.037.
23. Fodero-Tavoletti MT, Okamura N, Furumoto S, Mulligan RS, Connor AR, McLean CA, et al. 18F-THK523: a novel in vivo tau imaging ligand for Alzheimer's disease. Brain. 2011;134:1089–100. doi:10.1093/brain/awr038.
24. Okamura N, Furumoto S, Harada R, Tago T, Yoshikawa T, Fodero-Tavoletti M, et al. Novel 18F-labeled arylquinoline derivatives for noninvasive imaging of tau pathology in Alzheimer disease. J Nucl Med. 2013;54:1420–7. doi:10.2967/jnumed.112.117341.
25. Villemagne VL, Furumoto S, Fodero-Tavoletti MT, Mulligan RS, Hodges J, Harada R, et al. In vivo evaluation of a novel tau imaging tracer for Alzheimer's disease. Eur J Nucl Med Mol Imaging. 2014;41:816–26. doi:10.1007/s00259-013-2681-7.
26. Okamura N, Suemoto T, Furumoto S, Suzuki M, Shimadzu H, Akatsu H, et al. Quinoline and benzimidazole derivatives: candidate probes for in vivo imaging of tau pathology in Alzheimer's disease. J Neurosci. 2005;25:10857–62. doi:10.1523/JNEUROSCI.1738-05.2005.
27. Harada R, Okamura N, Furumoto S, Tago T, Maruyama M, Higuchi M, et al. Comparison of the binding characteristics of [18F]THK-523 and other amyloid imaging tracers to Alzheimer's disease pathology. Eur J Nucl Med Mol Imaging. 2013;40:125–32.
28. Okamura N, Furumoto S, Fodero-Tavoletti MT, Mulligan R, Harada R, Yates P, et al. Non-invasive assessment of Alzheimer's disease neurofibrillary pathology using 18F-THK5105 PET. Brain. 2014;137:1762–71.
29. Kitamoto T, Ogomori K, Tateishi J, Prusiner SB. Formic acid pretreatment enhances immunostaining of cerebral and systemic amyloids. Lab Invest. 1987;57:230–6.
30. Murayama H, Shin RW, Higuchi J, Shibuya S, Muramoto T, Kitamoto T. Interaction of aluminum with PHFtau in Alzheimer's disease neurofibrillary degeneration evidenced by desferrioxamine-assisted chelating autoclave method. Am J Pathol. 1999;155:877–85.
31. Verdurand M, Bort G, Tadino V, Bonnefoi F, Le Bars D, Zimmer L. Automated radiosynthesis of the Pittsburg compound-B using a commercial synthesizer. Nucl Med Commun. 2008;29:920–6. doi:10.1097/MNM.0b013e328304e0e1.
32. Muller-Gartner HW, Links JM, Prince JL, Bryan RN, McVeigh E, Leal JP, et al. Measurement of radiotracer concentration in brain gray matter using positron emission tomography: MRI-based correction for partial volume effects. J Cereb Blood Flow Metab. 1992;12:571–83. doi:10.1038/jcbfm.1992.81.
33. Whitwell JL, Josephs KA, Murray ME, Kantarci K, Przybelski SA, Weigand SD, et al. MRI correlates of neurofibrillary tangle pathology at autopsy: a voxel-based morphometry study. Neurology. 2008;71:743–9. doi:10.1212/01.wnl.0000324924.91351.7d.
34. Hof PR, Bierer LM, Perl DP, Delacourte A, Buee L, Bouras C, et al. Evidence for early vulnerability of the medial and inferior aspects of the temporal lobe in an 82-year-old patient with preclinical signs of dementia. Regional and laminar distribution of neurofibrillary tangles and senile plaques. Arch Neurol. 1992;49:946–53.
35. Kuzuhara S, Ihara Y, Toyokura Y, Shimada H. A semiquantitative study on Alzheimer neurofibrillary tangles demonstrated immunohistochemically with anti-tau antibodies, in the brains of non-demented and demented old people. No To Shinkei. 1989;41:465–70.
36. Price JL, Morris JC. Tangles and plaques in nondemented aging and "preclinical" Alzheimer's disease. Ann Neurol. 1999;45:358–68.
37. Morris JC, Price JL. Pathologic correlates of nondemented aging, mild cognitive impairment, and early-stage Alzheimer's disease. J Mol Neurosci. 2001;17:101–18.
38. Shoghi-Jadid K, Small GW, Agdeppa ED, Kepe V, Ercoli LM, Siddarth P, et al. Localization of neurofibrillary tangles and beta-amyloid plaques in the brains of living patients with Alzheimer disease. Am J Geriatr Psychiatry. 2002;10:24–35.
39. Small GW, Kepe V, Ercoli LM, Siddarth P, Bookheimer SY, Miller KJ, et al. PET of brain amyloid and tau in mild cognitive impairment. N Engl J Med. 2006;355:2652–63. doi:10.1056/NEJMoa054625.
40. Agdeppa ED, Kepe V, Liu J, Flores-Torres S, Satyamurthy N, Petric A, et al. Binding characteristics of radiofluorinated 6-dialkylamino-2-naphthylethylidene derivatives as positron emission tomography imaging probes for beta-amyloid plaques in Alzheimer's disease. J Neurosci. 2001;21:RC189.
41. Herholz K, Ebmeier K. Clinical amyloid imaging in Alzheimer's disease. Lancet Neurol. 2011;10:667–70. doi:10.1016/S1474-4422(11)70123-5.
42. Vandenberghe R, Van Laere K, Ivanoiu A, Salmon E, Bastin C, Triau E, et al. 18F-flutemetamol amyloid imaging in Alzheimer disease and mild cognitive impairment: a phase 2 trial. Ann Neurol. 2010;68:319–29. doi:10.1002/ana.22068.

Cortical Laminar Binding of PET Amyloid and Tau Tracers in Alzheimer Disease

Yi Li*[1,2], Wai Tsui[1], Henry Rusinek[1], Tracy Butler[1,3], Lisa Mosconi[1], Elizabeth Pirraglia[1], David Mozley[3], Shankar Vallabhajosula[3], Ryuichi Harada[4], Shozo Furumoto[5], Katsutoshi Furukawa[4], Hiroyuki Arai[4], Yukitsuka Kudo[4], Nobuyuki Okamura[4,6], and Mony J. de Leon*[1,7]

[1]Center for Brain Health, New York University, New York, New York; [2]Shandong University, Shandong, China; [3]Cornell University, Ithaca, New York; [4]Institute of Development, Aging, and Cancer, Sendai, Japan; [5]Cyclotron and Radioisotope Center, Sendai, Japan; [6]Tohoku University School of Medicine, Sendai, Japan; and [7]The Steven and Alexandra Cohen Veterans Center at NYU, New York, New York

Neurofibrillary tau pathology and amyloid β (Aβ) plaques, characteristic lesions of Alzheimer disease (AD), show different neocortical laminar distributions. Neurofibrillary-tangle tau pathology tends to be closer to the gray matter–white matter boundary, whereas Aβ is dispersed throughout the width of the cortical ribbon. **Methods:** Using PET radiotracers for tau and Aβ lesions, we developed an image analysis tool to measure the distance of tracer-positive voxels from the gray matter–white matter boundary. We studied 5 AD and 5 healthy subjects with both ^{18}F-THK5117 (tau) and ^{11}C-Pittsburgh compound B (Aβ) PET. **Results:** On average, tau-positive voxels were closer to the white matter than were Aβ-positive voxels. This effect was found for all AD subjects and for all regions, both before and after regionally adjusting for the nonspecific white matter binding of both tracers. The differential laminar pattern was validated through postmortem examination. **Conclusion:** Within cortical lamina, distance measures may be of value in testing PET tracers for their anatomic selectivity.

Key Words: tau; amyloid beta; neocortical binding; PET

J Nucl Med 2015; 56:270–273
DOI: 10.2967/jnumed.114.149229

Senile amyloid plaques and neurofibrillary tangles (tau pathology) are the two characteristic lesions required for a neuropathologic diagnosis of Alzheimer disease (AD) (*1*). On histopathology, amyloid β (Aβ) plaques are extracellular and dispersed throughout the neocortical ribbon (*2*). During the progression of AD, tau tangles initially appear in the hippocampal formation and subsequently in the neocortex (*3*), where they are intracellular and preferentially located in neocortical layers V and VI, closer to the gray matter–white matter boundary (*4*). Analogs of thioflavin T such as ^{11}C-Pittsburgh compound B (PiB) adapted for PET have been validated for imaging Aβ deposits (*5*). Recently, PET compounds have been developed to label tau pathology (*6–8*).

Typically, PET images are analyzed by assessing regional signal uptake in the cerebral cortex, but the distribution of signal within the cortical ribbon is ignored. The objective of this study was to investigate whether the differential spatial distributions of these two lesions in the cortical ribbon of AD patients can be detected with PET imaging. We tested the hypothesis that the bound tau tracer is closer to the gray matter–white matter boundary than is Aβ.

MATERIALS AND METHODS

Participants

Ten subjects were studied: 5 with probable AD (3 women and 2 men; mean age ± SD, 77.4 ± 13.0 y; range, 57–88 y; Mini-Mental State Examination score, 18.8 ± 5.9; Clinical Dementia Rating, 2.0 ± 1.0; education, 12.2 ± 3.6 y) and 5 healthy elderly controls (4 men and 1 woman; mean age, 71.6 ± 4.2 y; range, 67–78 y; Mini-Mental State Examination score, 28.8 ± 1.8; Clinical Dementia Rating, 0; education, 13.6 ± 2.2 y). Written informed consent was obtained from all participants. One AD postmortem autoradiography validation study was conducted using ^{3}H-THK5117 and ^{3}H-PiB. The protocol was approved by the Ethics Committee of Tohoku University Hospital. Controls were recruited by advertisements in the community. AD patients were recruited from the memory clinic of Tohoku University Hospital. The clinical and neuropsychological performance of the participants was assessed by a neurologist and a neuropsychologist in consensus, who were not aware of the PET results. AD was diagnosed according to the criteria of the National Institute of Neurologic and Communicative Disorders and Stroke/Alzheimer's Disease and Related Disorders Association.

Image Acquisition

MR imaging was performed on a SIGNA 1.5-T magnet (GE Healthcare). A 3-dimensional volumetric acquisition of a T1-weighted spoiled gradient recalled sequence produced gapless axial sections (echo time/repetition time, 2.4/50 ms; flip angle, 45°; acquisition matrix, 256 × 256; 1 excitation; field of view, 22 cm; slice thickness, 2.0 mm). The two radiotracers, 6-[(3-^{18}F-fluoro-2-hydroxy)propoxy]-2-(4-methylaminophenyl)quinoline (^{18}F-THK5117) and ^{11}C-PiB, were prepared at the Cyclotron and Radioisotope Center of Tohoku University. ^{18}F-THK5117 was synthesized as described previously (*9*). ^{11}C-PiB PET was synthesized using the 1-step ^{11}C-methyl triflate approach (*10*). PET data were acquired using an Eminence STARGATE PET scanner (Shimadzu) from 0 to 90 min for ^{18}F-THK5117 with a dosage of 185 mBq and from 0 to 70 min for ^{11}C-PiB with dosage of 296 mBq.

Received Sep. 30, 2014; revision accepted Dec. 11, 2014.
For correspondence or reprints contact: Mony J. de Leon, NYU School of Medicine, Department of Psychiatry,145 E. 32 St., 5th Floor, New York, NY 10016.
E-mail: mony.deleon@nyumc.org.
*Contributed equally to this work.
Published online Jan. 15, 2015.

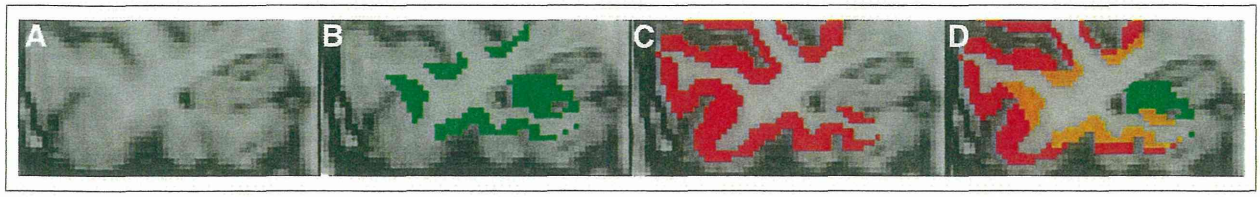

FIGURE 1. (A) T1-weighted MR image of right temporal cortex of AD patient. (B) Tau-positive voxels (green). (C) Amyloid-positive voxels (red). (D) Overlapping tau and amyloid voxels (orange). All are at 1.5-SD cutoff.

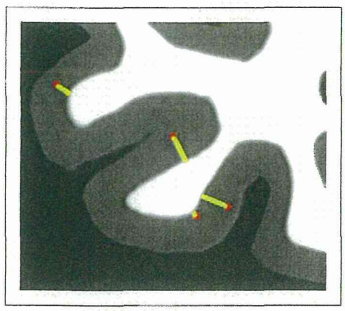

FIGURE 2. Schematic representation of distance[v] image. For each PET tracer, positive gray ribbon voxels (red dots) were defined by statistical threshold and shortest distance to white matter boundary computed (yellow line). Gray matter ribbon and gray matter–white matter boundary are defined by MR imaging.

Image Analysis

For each subject, dynamic PET frames of both ^{18}F-THK5117 and ^{11}C-PiB were realigned using SPM8 software (www.fil.ion.ucl.ac.uk/spm). Standardized uptake value (SUV) images were generated from ^{18}F-THK5117 using the 50- to 80-min frames and from ^{11}C-PiB using the 50- to 70-min frames. All SUV images were coregistered to the corresponding MR imaging volumes using SPM8. MR imaging–determined regions of interest were used to sample the PET images. MR imaging–based regions of interest were determined by Free-Surfer (version 5.1, http://surfer.nmr.mgh.harvard.edu) for the gray and white matter for the entire neocortex (principal outcome) and separately for the frontal, parietal, occipital, and temporal lobes and for the cerebellum. For each tracer, the cerebellar gray matter was used to create regional SUV ratios (SUVRs).

Cutoff cortex values for positive and negative ^{18}F-THK5117 and ^{11}C-PiB PET voxels were regionally defined referencing the mean control SUVR and SD. Cutoffs were tested at 1.5 (Fig. 1) and 1.0 times the SD. A distance[v] measure was generated for all positive cortical voxels for each tracer based on the shortest distance to the MR imaging–defined gray matter–white matter boundary (Fig. 2). To test whether distance[v] distinguished ^{18}F-THK5117 binding from ^{11}C-PiB binding, the distributions in AD subjects were estimated for each of the regions of interest. Voxels located in the neocortex with an apparent thickness of less than 1.0 mm (likely caused by segmentation errors, <10% of total) were excluded from the analysis.

Statistical Analysis

We tested the hypothesis that distance[v] is shorter for tau than for Aβ by the paired *t* test and the nonparametric Wilcoxon signed-rank test. A residual approach was taken to adjust for the confounding effects of nonspecific white matter uptake of the two tracers. Specifically, in the control group, regional regression equations defining the relationships between distance[v] and adjacent white matter uptake were estimated. Subsequently, these regression models were applied to the AD group and used to calculate the AD residuals (residual = actual value minus predicted value). The residuals and actual values were tested. Analyses were performed with SPSS, version 19 (IBM). Results were declared statistically significant when *P* was less than 0.05.

RESULTS

Compared with controls (C), the total neocortex SUVR was higher in AD for both ^{11}C-PiB ($\bar{x}_{SUVR\text{-}C}$ = 1.13 ± 0.04, $\bar{x}_{SUVR\text{-}AD}$ = 1.69 ± 0.17) and ^{18}F-THK5117 ($\bar{x}_{SUVR\text{-}C}$ = 1.12 ± 0.06, $\bar{x}_{SUVR\text{-}AD}$ = 1.31 ± 0.07). The average cortical thickness was 1.90 mm in AD patients and 2.85 mm in controls. For both the 1.5- and the 1.0-SD cutoffs, in all regions the mean distance[v] was significantly shorter for tau than for Aβ. Adjustment for partial-volume artifacts did not change the results (Table 1). All significant test results were confirmed using the Wilcoxon signed-rank test. Figure 1 shows the AD spatial distribution of tau and Aβ tracer binding in the temporal lobe of a representative patient. The individual distance[v] data are in the supplemental data (available online at http://jnm.snmjournals.org).

TABLE 1
Mean Distance[v] and Total Counts for ^{18}F-THK5117– and ^{11}C-PiB–Positive Voxels (1.5-SD Cutoff)

Region	^{18}F-THK5117 (mm)	^{11}C-PiB (mm)	Unadjusted *P*	Regression-adjusted *P*	Number of positive voxels (×10^5)	
					^{18}F-THK	^{11}C-PiB
Total cortex	1.49 ± 0.11	1.73 ± 0.10	0.01	0.02	2.2	11.1
Frontal cortex	1.42 ± 0.06	1.78 ± 0.15	0.01	0.04	0.6	4.3
Parietal cortex	1.32 ± 0.05	1.50 ± 0.05	0.01	0.04	0.4	2.5
Temporal cortex	1.70 ± 0.23	1.89 ± 0.19	0.01	0.01	0.7	2.1
Occipital cortex	1.44 ± 0.13	1.66 ± 0.06	0.01	0.01	0.2	1.0

Data are mean ± SD.

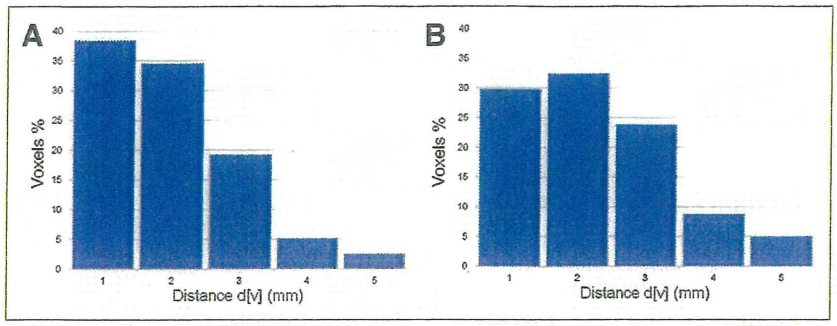

FIGURE 3. AD distance[v] histogram for neocortical ^{18}F-THK5117– and ^{11}C-PiB–positive voxels (1.5 SDs). (A) Distance[v] histogram of ^{18}F-THK5117–positive voxels in total neocortex. (B) Distance[v] histogram of ^{11}C-PiB–positive voxels in total neocortex.

For ^{11}C-PiB at the 1.5-SD cutoff, the total number of positive voxels (1.1×10^6) was approximately 5 times greater than that for ^{18}F-THK5117 (0.2×10^6). Histogram analysis of the neocortical distribution pattern of ^{11}C-PiB– and ^{18}F-THK5117–positive voxels showed that ^{18}F-THK5117 skewed toward shorter distances (Fig. 3). This distribution pattern was not observed in controls (Supplemental Fig. 1).

The postmortem autoradiography study also showed that tau binding localized to the deeper cortical layers, whereas ^{11}C-PiB binding was more widely distributed (Fig. 4).

DISCUSSION

Previous studies have shown a diagnostic value for PiB (*5*) and for THK5117 (*8*) in AD. However, the intralaminar distributions of THK5117 and PiB have not been previously described. In agreement with neuropathologic evidence that tau and Aβ, the principal lesions of AD, have different cortical laminar distributions (*4*), we present the first (to our knowledge) PET imaging confirmation of this distribution pattern. Neurofibrillary pathology in AD is typically found in the deeper cortical lamina whereas plaques are widely distributed (2,4). In agreement, we found with PET that the average distance[v] of tau-positive cortical voxels to the gray matter–white matter boundary is shorter than that of Aβ-positive voxels. We observed this effect in each AD subject and for all regions tested. These PET findings are further supported by our postmortem study using THK5117 and PiB to map Aβ and tau pathology.

Although the distance[v] difference between the imaged tau and Aβ deposits was approximately 0.2 mm, well below the spatial resolution of PET (*11*), because of the large number ($\sim 10^6$) of voxels the effect was significant and observed in all 5 AD patients and in all brain regions. When measured with the Cohen κ (the mean difference between the ^{11}C-PiB and ^{18}F-THK5117 distances, divided by overall SD), the effect was nearly 200%.

Our finding of a 5-fold increased magnitude of Aβ over tau-positive voxels indicates the greater extent of Aβ pathology. These findings are also consistent with neuropathologic findings (*12*) and further contribute to the face validity of PET imaging in AD.

Cross-contamination between adjacent cortical and white matter voxels, each with distinct tracer uptake, is referred to as the partial-volume artifact. To investigate whether our findings can be attributed to this artifact, we generated a conservative control-group–based model that regresses the lesion distance measure on the white matter SUVR. After applying the adjustment to the AD group, the tracer pattern remained significant for all brain regions at the conservative 1.5-SD lesion cutoff.

The current method is of potential interest for subjects experiencing traumatic brain injury, for whom the laminar distribution of the tau pathology is reported to be more superficial (*13*). Future studies will also examine continuous measures of tracer retention, with distance being weighted by the uptake in each voxel.

CONCLUSION

PET images of AD subjects show different laminar distributions of tau and Aβ deposits. Tau pathology tends to localize in the deeper lamina of the cortical ribbon, whereas the Aβ is more uniformly distributed. This observation may lead to a new biomarker of AD progression. It may also be of use in the evaluation of other neurodegenerative disorders with different tau distributions.

DISCLOSURE

The costs of publication of this article were defrayed in part by the payment of page charges. Therefore, and solely to indicate this fact, this article is hereby marked "advertisement" in accordance with 18 USC section 1734. Work at NYU was supported by

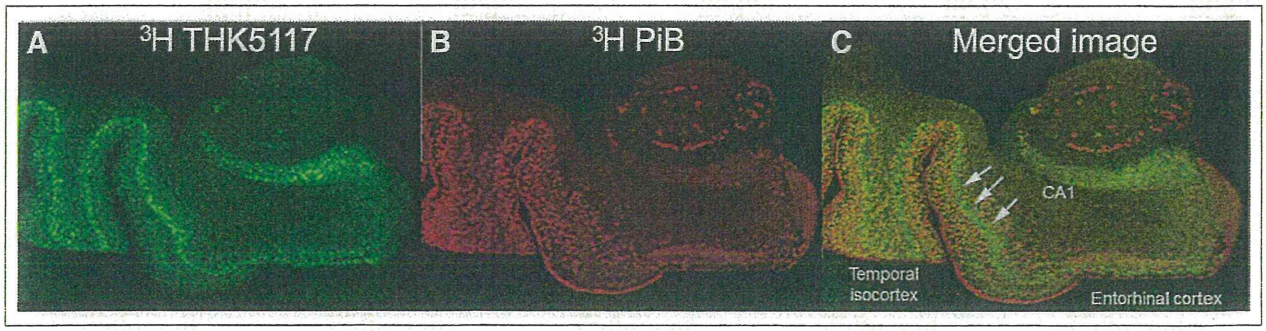

FIGURE 4. AD autoradiography images: ^{3}H-THK5117 (green) (A), ^{3}H-PiB (red) (B), and overlapping tau and amyloid binding (orange) (C). Arrows highlight more inferior tau pathology distribution.

NIH/NIA grants AG035137, AG032554, AG022374, AG013616, and AG012101 and by the Steven and Alexandra Cohen Veterans Center. Work at Tohoku University was supported by Health and Labor Sciences research grants from the Ministry of Health, Labor, and Welfare of Japan, a Grant-in-Aid for Scientific Research (B) (23390297), a Grant-in-Aid for Scientific Research on Innovative Areas (26117003), a grant from the Japan Advanced Molecular Imaging Program (J-AMP) of the Ministry of Education, Culture, Sports, Science and Technology, and the research fund from GE Healthcare and Sumitomo Electric Industries, Ltd. No other potential conflict of interest relevant to this article was reported.

ACKNOWLEDGMENT

Yi Li is a PhD student at Shandong University. This work partially fulfills Yi Li's PhD degree requirements. Both Shandong University and New York University are primary affiliations of Yi Li.

REFERENCES

1. Hyman BT, Trojanowski JQ. Consensus recommendations for the postmortem diagnosis of Alzheimer disease from the National Institute on Aging and the Reagan Institute working group on diagnostic criteria for the neuropathological assessment of Alzheimer disease. *J Neuropathol Exp Neurol.* 1997;56:1095–1097.
2. Thal DR, Rub U, Orantes M, Braak H. Phases of A beta-deposition in the human brain and its relevance for the development of AD. *Neurology.* 2002;58:1791–1800.
3. Braak H, Braak E. Neuropathological stageing of Alzheimer-related changes. *Acta Neuropathol.* 1991;82:239–259.
4. Hof PR, Bouras C, Buee L, Delacourte A, Perl DP, Morrison JH. Differential distribution of neurofibrillary tangles in the cerebral cortex of dementia pugilistica and Alzheimer's disease cases. *Acta Neuropathol.* 1992;85:23–30.
5. Klunk WE, Engler H, Nordberg A, et al. Imaging brain amyloid in Alzheimer's disease with Pittsburgh compound-B. *Ann Neurol.* 2004;55:306–319.
6. Chien DT, Szardenings AK, Bahri S, et al. Early clinical PET imaging results with the novel PHF-tau radioligand [F18]-T808. *J Alzheimers Dis.* 2014;38:171–184.
7. Okamura N, Furumoto S, Fodero-Tavoletti MT, et al. Non-invasive assessment of Alzheimer's disease neurofibrillary pathology using ^{18}F-THK5105 PET. *Brain.* 2014;137:1762–1771.
8. Ishiki A, Furumoto S, Harada R, et al. Accumulation of the novel tau imaging tracer ^{18}F-THK-5117 is associated with brain atrophy in Alzheimer's disease [abstract]. *Alzheimers Dement.* 2014;10(suppl):P131.
9. Okamura N, Furumoto S, Harada R, et al. Novel ^{18}F-labeled arylquinoline derivatives for noninvasive imaging of tau pathology in Alzheimer disease. *J Nucl Med.* 2013;54:1420–1427.
10. Rowe CC, Ng S, Ackermann U, et al. Imaging beta-amyloid burden in aging and dementia. *Neurology.* 2007;68:1718–1725.
11. Rahmim A, Qi J, Sossi V. Resolution modeling in PET imaging: theory, practice, benefits, and pitfalls. *Med Phys.* 2013;40:064301.
12. Mungas D, Tractenberg R, Schneider JA, Crane PK, Bennett DA. A 2-process model for neuropathology of Alzheimer's disease. *Neurobiol Aging.* 2014;35:301–308.
13. Baugh CM, Stamm JM, Riley DO, et al. Chronic traumatic encephalopathy: neurodegeneration following repetitive concussive and subconcussive brain trauma. *Brain Imaging Behav.* 2012;6:244–254.

Eur J Nucl Med Mol Imaging (2014) 41:816–826
DOI 10.1007/s00259-013-2681-7

ORIGINAL ARTICLE

In vivo evaluation of a novel tau imaging tracer for Alzheimer's disease

Victor L. Villemagne · Shozo Furumoto · Michelle T. Fodero-Tavoletti · Rachel S. Mulligan · John Hodges · Ryuichi Harada · Paul Yates · Olivier Piguet · Svetlana Pejoska · Vincent Doré · Kazuhiko Yanai · Colin L. Masters · Yukitsuka Kudo · Christopher C. Rowe · Nobuyuki Okamura

Received: 14 October 2013 / Accepted: 20 December 2013 / Published online: 11 February 2014

Abstract
Purpose Diagnosis of tauopathies such as Alzheimer's disease (AD) still relies on post-mortem examination of the human brain. A non-invasive method of determining brain tau burden in vivo would allow a better understanding of the pathophysiology of tauopathies. The purpose of the study was to evaluate ^{18}F-THK523 as a potential tau imaging tracer.

Methods Ten healthy elderly controls, three semantic dementia (SD) and ten AD patients underwent neuropsychological examination, MRI as well as ^{18}F-THK523 and ^{11}C-Pittsburgh compound B (PIB) positron emission tomography (PET) scans. Composite memory and non-memory scores, global and hippocampal brain volume, and partial volume-corrected tissue ratios for ^{18}F-THK523 and ^{11}C-PIB were estimated for all participants. Correlational analyses were performed between global and regional ^{18}F-THK523, ^{11}C-PIB, cognition and brain volumetrics.
Results ^{18}F-THK523 presented with fast reversible kinetics. Significantly higher ^{18}F-THK523 retention was observed in the temporal, parietal, orbitofrontal and hippocampi of AD patients when compared to healthy controls and SD patients. White matter retention was significantly higher than grey matter retention in all participants. The pattern of cortical ^{18}F-THK523 retention did not correlate with Aβ distribution as assessed by ^{11}C-PIB and followed the known distribution of tau in the AD brain, being higher in temporal and parietal areas than in the frontal region. Unlike ^{11}C-PIB, hippocampal ^{18}F-THK523 retention was correlated with several cognitive parameters and with hippocampal atrophy.
Conclusion ^{18}F-THK523 does not bind to Aβ in vivo, while following the known distribution of paired helical filaments (PHF)-tau in the brain. Significantly higher cortical ^{18}F-THK523 retention in AD patients as well as the association of hippocampal ^{18}F-THK523 retention with cognitive parameters and hippocampal volume suggests ^{18}F-THK523 selectively binds to tau in AD patients. Unfortunately, the very high ^{18}F-THK523 retention in white matter precludes simple visual inspection of the images, preventing its use in research or clinical settings.

Keywords Alzheimer's disease · Tau imaging · Aβ Imaging · Neurodegeneration · Brain

Electronic supplementary material The online version of this article (doi:10.1007/s00259-013-2681-7) contains supplementary material, which is available to authorized users.

V. L. Villemagne · M. T. Fodero-Tavoletti · R. S. Mulligan · P. Yates · S. Pejoska · V. Doré · C. C. Rowe
Centre for PET, Austin Health, Melbourne, Australia

V. L. Villemagne · M. T. Fodero-Tavoletti · C. L. Masters
The Mental Health Research Institute, Melbourne, Australia

S. Furumoto · R. Harada · K. Yanai · N. Okamura
Department of Pharmacology, Tohoku University School of Medicine, Sendai, Japan

J. Hodges · O. Piguet
Neuroscience Research Australia, Sydney, Australia

J. Hodges · O. Piguet
The University of New South Wales, Sydney, Australia

V. Doré
Preventative Health Flagship, CSIRO ICT, Brisbane, Australia

Y. Kudo
Innovation of New Biomedical Engineering Center, Tohoku University, Sendai, Japan

V. L. Villemagne (✉)
Department of Nuclear Medicine and Centre for PET, Austin Health, 145 Studley Rd, Heidelberg, VIC 3084, Australia
e-mail: villemagne@petnm.unimelb.edu.au

Introduction

Most neurodegenerative conditions are characterized by the aggregation of a misfolded protein such as Aβ and tau in Alzheimer's disease (AD), transactive response (TAR) DNA binding protein 43 kDa (TDP-43) in some forms of frontotemporal lobar degeneration (FTLD) such as semantic dementia (SD) or α-synuclein in Parkinson's disease. Tauopathies are neurodegenerative diseases characterized by the pathological accumulation of aggregated tau. AD is the most common tauopathy and the leading cause of dementia [1], but tau deposits are also found in other variants of FTLD, such as progressive non-fluent aphasia (PNFA) or in some cases of behavioural frontotemporal dementia (bFTD) [2]. Other tauopathies include Down's syndrome, Guam parkinsonism-dementia complex, frontotemporal dementia with parkinsonism linked to chromosome 17, corticobasal degeneration, progressive supranuclear palsy and chronic traumatic encephalopathy [3–5]. Definitive diagnosis of these neurodegenerative conditions can only be established after death. While these tauopathies share tau immunoreactivity in post-mortem brain examination, these tau aggregates can be composed of different tau isoforms displaying very distinct histopathological and ultrastructural differences [3, 6, 7]. In AD, these tau deposits can be recognized histologically as neurofibrillary tangles (NFTs) and neuropil threads as well as dystrophic neurites in senile plaques, whilst ultrastructurally they aggregate in paired helical filaments (PHF) [3, 4, 8]. While the underlying mechanisms leading to tau hyperphosphorylation, misfolding and aggregation remain unclear, tau aggregation and deposition follows a stereotypical and spatiotemporal pathway both at the intraneuronal level [8, 9] as well as in its topographical and neuroanatomical distribution in the brain [4, 10, 11].

The notion that tau dysregulation is a key mediator of neurodegeneration [12, 13] has stimulated the development of therapeutics for the treatment of AD and non-AD tauopathies [14–16]. Given these treatments are currently being developed, a non-invasive method of determining the tau burden in the brain would allow a better understanding of the pathophysiology of AD, FTLD and other tau-related neurodegenerative conditions. It will also lead to improvements in differential diagnostic accuracy and accelerate drug discovery by facilitating patient selection and monitor efficacy in novel anti-tau therapeutic trials. It would assist in the early and differential diagnosis of AD and non-AD tauopathies, while helping ascertain the relationship between the spatiotemporal distribution of tau aggregates in the brain to cognition and brain volumetrics. Development of tau imaging probes poses several more challenges than those associated with Aβ imaging, and these are mainly related to the idiosyncrasies of tau aggregation and deposition. In contrast to Aβ, most tau aggregates are intracellular, there are six tau isoforms and the different combinations of these isoforms manifest as different clinical phenotypes. Tau aggregates undergo a wide spectrum of post-translation modifications that, in addition to the combination of different isoforms, lead to diverse ultrastructural conformations and typical pathological lesions. Furthermore, tau aggregates coexist with other misfolded proteins sharing the same β-sheet secondary structure, as is in the case of AD where tau and Aβ are both co-localized in grey matter areas, where the concentrations of Aβ are, depending on the brain region, ~5–20 times higher than those of tau (for an in depth review see Villemagne et al. [17]).

In recent years, the main focus has been the development of selective ligands that allow early detection of Aβ deposition [18]. Among these tracers, ^{18}F-FDDNP was reported to non-selectively bind to both Aβ deposits and NFTs [19]. Phenylquinoline derivatives binding with high affinity and selectivity for tau aggregates have been developed as candidates for tau imaging agents at Tohoku University in Sendai, Japan [20]. Among them, ^{18}F-THK523 (THK523) was the first reported selective tau imaging tracer that can non-invasively detect tau deposits in a transgenic mouse brain [21]. This report was recently followed by several other potential tau tracer candidates [22–27].

After a careful in vitro evaluation, the initial in vivo characterization of a novel positron emission tomography (PET) neuroligand candidate requires to fulfill certain conditions such as safety at low tracer doses, possess high affinity and selectivity for the target, ability to cross the blood–brain barrier, display low non-specific binding with adequate regional distribution and its relation to parameters known to be associated with the intended target, suitable brain kinetics, lack of problematic radiolabelled metabolites [28] before it is applied to research or clinical use (Supplementary Fig. 1).

Therefore, the main objective of the present study was to characterize the in vivo suitability of THK523 for tau imaging in humans. The in vivo assessment comprised: (a) comparing the global and regional THK523 binding in healthy controls (HC), AD and SD patients, (b) assessing the relationship between THK523 retention and cognition, (c) assessing the relationship between THK523 retention and brain volumetrics and (d) comparing the regional brain distribution of THK523 with that of ^{11}C-Pittsburgh compound B (PIB) in the same participants.

Materials and methods

Participants

Written informed consent was obtained from all participants. Approval for the study was obtained from the Austin Health Human Research Ethics Committee. Elderly HC were recruited by advertisement in the community and dementia patients

were recruited from tertiary Memory Disorders Clinics or from physicians who sub-specialize in dementia care. All participants were classified on the basis of their clinical and neuropsychological performance by consensus of a neurologist and a neuropsychologist. Individuals classified as HC performed within normal limits on cognitive tests. AD patients met NINCDS-ADRDA criteria for probable AD [29], while three FTLD patients were classified as SD [30, 31]. None of the AD or FTLD patients had a family history of dementia.

Safety evaluation

Clinical, haematological and biochemical data on the safety of THK523 were collected for all participants. Heart rate, blood pressure, temperature and respiratory rate were measured immediately prior to injection and at 2, 15, 60 and 180 min post-injection. Immediately prior to THK523 injection, blood was drawn for routine haematology and biochemistry tests. An ECG was performed prior to injection of THK523 and at the completion of the scan, when they were also questioned for adverse events. All subjects were contacted by telephone 24 h later and questioned for adverse events. Between 5 and 8 days post-injection, subjects returned to be questioned for adverse events and for a physical examination, including a set of observations and repeat haematology and biochemistry testing.

Neuropsychological evaluation

In addition to the Mini-Mental State Examination (MMSE), Clinical Dementia Rating (CDR) and Clinical Dementia Rating Sum of Boxes (CDR SOB), the primary cognitive performance measures were composite episodic memory and non-memory scores generated as previously described [32]. Briefly, a composite episodic memory score was calculated by taking the average of the z scores (generated using 65 HC with both low PIB and normal MRI as the reference) for Rey Complex Figure Test (RCFT, 30 min) Long Delay and California Verbal Learning Test - Second Edition (CVLT-II) Long Delay and Logical Memory II. A composite non-memory score was calculated by taking the average of the z scores for the Boston Naming Test, letter fluency, category fluency, digit span forwards and backwards, digit symbol-coding and RCFT copy.

Image acquisition

Magnetic resonance imaging

Participants received an MRI on a 3 T Siemens TRIO MRI system (Siemens Healthcare, Erlangen, Germany) using the Alzheimer's Disease Neuroimaging Initiative (ADNI) 3D magnetization prepared rapid acquisition gradient echo (MPRAGE) sequence with 1×1 mm in-plane resolution and 1.2-mm slice thickness, repetition time (TR)/echo time (TE)/T1-weighted=2,300/2.98/900, flip angle 9° and field of view 240×256 and 160 slices. T2 -weighted fast spin-echo (FSE) and fluid-attenuated inversion recovery (FLAIR) sequences were also obtained. The interval between the THK523 and MRI studies was 1.6±3.3 months.

Positron emission tomography

Productions of ^{11}C-PIB and ^{18}F-THK523 were performed in the Centre for PET, Austin Hospital. ^{11}C-PIB was synthesized using the one-step ^{11}C-methyl triflate approach as previously described [18]. The decay-corrected average radiochemical yield for ^{11}C-PIB was 30 % with a radiochemical purity of >98 % and a specific activity of 30±7. 5 GBq/μmol. ^{18}F-THK523 was synthesized by nucleophilic substitution of the tosylate precursor [BF-241, 2-3 mg in 700 μl dimethyl sulphoxide (DMSO)]. The decay-corrected average radiochemical yield of the production of ^{18}F-THK523 was 22.5± 5 %, with a radiochemical purity of>95 % and a specific activity of 225.6±134.8 GBq/μmol (6.2±3.3 Ci/μmol).

A 30-min acquisition (6×5-min frames) on an Allegro™ PET camera started 40 min after injection of 300 MBq ^{11}C-PIB intravenously. A 90-min list-mode emission acquisition was performed in 3D mode after injection of 200 MBq ^{18}F-THK523. List-mode raw data were sorted offline into 6×30-s, 7×1-min, 4×2.5-min, 2×5-min and 6×10-min frames. The sorted sinograms were reconstructed using a 3D row action maximum likelihood algorithm (RAMLA). The interval between the THK523 and PIB PET studies was 0.3±3.8 months.

Tracer metabolism

Compound stability was assessed by incubating the tracer for 5, 30, 60, 90, 180 and 240 min with human S9 liver fractions.

Image analysis

Magnetic resonance imaging

Hippocampal and cortical grey matter volumes were obtained using a commercial fully automated volumetric measurement program (NeuroQuant®) applied to the 3D MPRAGE MRI images. The primary MRI performance measures were the grey cortical matter and hippocampal volumes normalized for total intracranial volume.

Positron emission tomography

PET images were processed using a semi-automatic region of interest (ROI) method as previously described [32]. Briefly,

THK523 and PIB PET images were co-registered to each individual's MRI using SPM8 (Wellcome Trust Centre for Neuroimaging, London, UK), and the same ROI template was applied. Given the reversible nature of THK523 kinetics, distribution volume ratios (DVR) were determined through graphical analysis of the dynamic data. Standardized uptake value ratios (SUVR) for PIB and THK523 as well as THK523 DVR were generated using the cerebellar cortex as reference region [18, 33]. Global tau and Aβ burden were expressed as the average SUVR for the following cortical ROIs: frontal (consisting of dorsolateral prefrontal, ventrolateral prefrontal and orbitofrontal regions), superior parietal, lateral temporal, lateral occipital and anterior and posterior cingulate for THK523 and PIB, respectively. As in previous studies, a PIB SUVR threshold of 1.5 was used to categorize high (PIB+) and low (PIB−) Aβ burden [32].

Partial volume correction (PVC), accounting for *both* grey matter atrophy and white matter spillover, was performed applying a three-compartment approach using PMOD 3.1 (PMOD Technologies Ltd., Zurich, Switzerland). DVR for THK523 were determined through graphical analysis of the last 45 min of the 90-min acquisition [33]. In order to avoid arterial blood sampling, a simplified approach was applied using the cerebellar cortex as reference region [18, 33]. Global DVR was calculated with the same regions used for the global SUVR. The primary outcome measure used for all THK523 and PIB assessments was the PVC SUVR.

Statistical evaluation

Normality of distribution was tested using the Shapiro-Wilk test and visual inspection of variable histograms. Statistical evaluations to establish differences between clinical groups means were performed using a Tukey-Kramer HSD test and by a Dunnett's test to compare each group with controls. Pearson's product-moment correlation analyses were conducted between imaging and clinical variables. Categorical differences were evaluated using Fisher's exact test. Effect size was measured with Cohen's *d*. All analyses were adjusted for age and corrected for multiple comparisons using false discovery rates. Data are presented as mean±standard deviation unless otherwise stated.

Results

Participants

Demographic characteristics of the participants are shown in Table 1. As expected, there were significant differences between the AD and SD patients and HC in cognitive performance and brain volumetrics. The AD group also presented with significantly higher PIB retention. While there were no significant differences between groups in age and gender, the AD group was less educated. While seven of the HC and the three SD patients showed low PIB retention, three of the HC presented with high PIB retention (Table 1).

No adverse events related to the study drug were observed or reported by participants or carers following the THK523 scan. There were no significant changes in clinical or biochemical parameters.

Tracer metabolism

THK523 was minimally metabolized, with 91, 81 and 65 % of unchanged parent compound remaining at 30, 90 and 180 min, respectively. No lipophilic radiometabolites were observed.

Brain kinetics

Brain THK523 radioactivity peaked between 3 and 6 min post-injection and the binding appeared to be reversible with rapid clearance from the brain (Fig. 1a, b). THK523 cleared fastest from cerebellar cortex and the clearance rate was the same for all groups (Fig. 1a, b). Clearance was slower from cortical areas in AD (Fig. 1b) than in HC (Fig. 1a) and SD patients. The ratio of cortical to cerebellar binding became constant in all participants by 50 min after injection (Fig. 1c).

Visual inspection

Visual inspection of the summed 60–90-min SUVR images revealed significantly higher THK523 retention in white matter than in grey matter regions, being significantly higher in AD patients than in HC or SD (Fig. 1d).

Assessment of tau burden

Regional analysis showed that there were no group differences in cerebellar cortex THK523 SUV, and there was no correlation between cerebellar cortex THK523 SUV with age in the whole cohort or with dementia severity in the AD group as assessed by MMSE (r=0.25, p=0.50), CDR (r=0.13, p=0.72) or CDR SOB (r=0.03, p=0.94).

While 60–90-min THK523 SUVR was estimated for all participants, four participants (two HC and two AD) were not able to complete the initial THK523 dynamic scan preventing calculation of DVR. In the remaining 16 subjects, significantly higher THK523 DVR were found in AD subjects in all cortical regions. The global THK523 DVR was 1.02±0.15 in AD vs 0.86±0.11 in HC (p=0.04, Cohen's effect size d=1.2). No significant differences were observed between HC and SD patients. Similar findings were observed with THK523

Table 1 Demographics

	HC (n=10)	SD (n=3)	AD (n=10)
Age	77.4±10.0	65.6±8.1	75.6±9.5
Gender (M/F)	3/7	1/2	4/6
MMSE	29.3±1.1	21.7±1.2*	16.7±6.6*
CDR	0.0	0.8±0.3*	1.3±0.6*
CDR SOB	0.1±0.2	2.5±1.1*	7.3±4.5*
Years of education	14.7±2.7	12.5±4.9	11.5±3.6*
Episodic memory scores	−0.4±0.6	−1.9±0.9*	−3.8±0.5*
Non-memory scores	−0.1±0.4	−1.4±1.2*	−3.4±1.6*
Hippocampal volume (cm^3)	5.1±0.6	4.3±0.3	4.1±1.0*
Aβ burden (PIB SUVR)	1.5±0.6	1.1±0.1	2.9±0.5*
	[PIB−=1.2±0.1 (n=7)]		
	[PIB+=2.2±0.6 (n=3)]		

MMSE Mini-Mental State Examination, *CDR* Clinical Dementia Rating, *CDR SOB* Clinical Dementia Rating Sum of Boxes, *PIB* Pittsburgh compound B, *SUVR* standardized uptake value ratio, *PIB−* low PIB retention, *PIB+* high PIB retention

*Significantly different from HC (p<0.05)

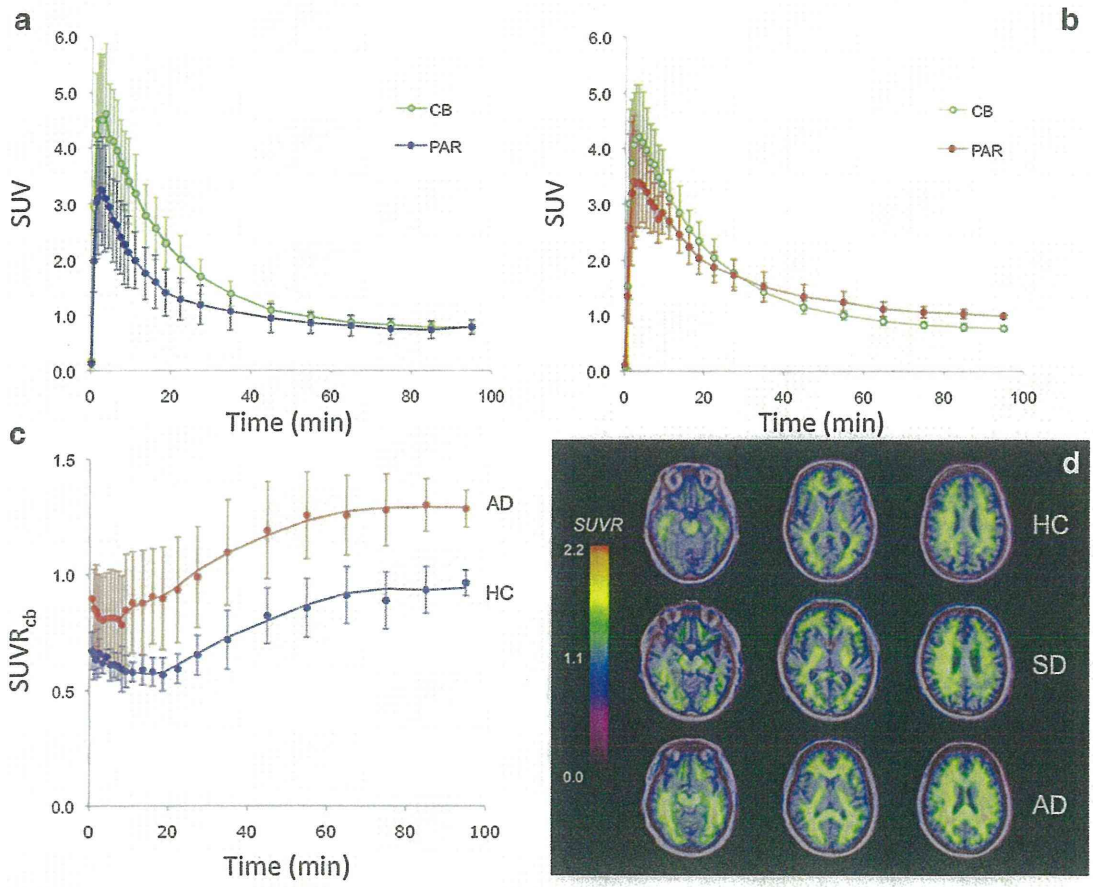

Fig. 1 ^{18}F-THK523 binding. Time-radioactivity curves for ^{18}F-THK523 in the parietal cortex (*PAR*) and the cerebellar grey matter (*CB*) in healthy controls (*HC*) (**a**) and Alzheimer's disease (*AD*) patients (**b**). There is fast ^{18}F-THK523 uptake in the brain followed by a fast clearance phase. While there is slower clearance with significantly higher retention in the parietal cortex of AD patients compared to HC, there are no significant differences in the cerebellar cortex uptake and clearance, further validating its use as reference region. **c** The total to non-specific binding ratios curves show significantly higher ^{18}F-THK523 retention in the parietal cortex of AD patients compared to HC. The specific binding reaches a plateau by 50 min post-injection. **d** Representative ^{18}F-THK523 PET images at three different brain levels in a 69-year-old female HC (MMSE 30, *top row*), a 73-year-old male semantic dementia (*SD*) patient (MMSE 21, *middle row*) and a 72-year-old female AD patient (MMSE 22, *bottom row*). Visual inspection of the images reveals no differences in ^{18}F-THK523 retention between HC and SD. There is higher white matter retention in AD compared to HC and SD. Data expressed as mean±SD of ten HC and ten AD patients

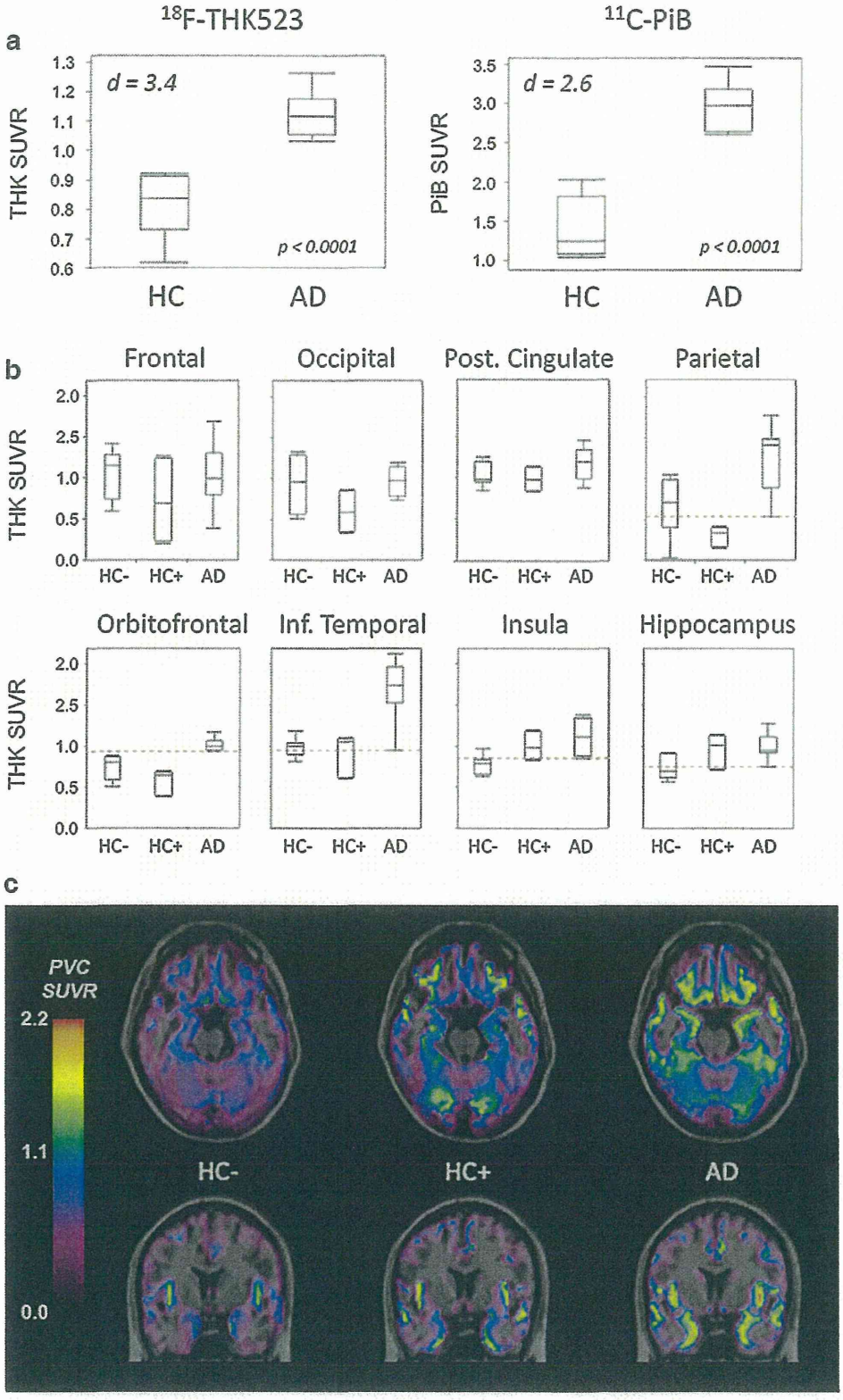

SUVR, and although SUVR values were higher than THK523 DVR, the rank order of the participants and the rank order of the regional values were identical, both showing the highest THK523 retention in temporal, parietal and hippocampus.

Table 2 Global and regional ^{18}F-THK523 and ^{11}C-PIB retention in AD

Region	THK SUVR				PIB SUVR			
	HC	AD	*p*	*d*	HC	AD	*p*	*d*
Frontal lobe	0.92±0.38	1.01±0.36	0.56	0.24	1.51±0.74	3.05±0.68	<0.0001	2.17
Orbitofrontal	0.68±0.16	1.06±0.24	<0.0001	1.87	1.42±0.50	2.91±0.58	<0.0001	2.74
Ant. cingulate	0.60±0.45	0.54±0.22	0.52	−0.19	1.61±0.75	2.98±0.59	<0.0001	2.04
Post. Cingulate	0.99±0.15	1.17±0.20	0.029	1.02	1.57±0.65	3.39±0.49	<0.0001	3.16
Parietal lobe	0.54±0.33	1.24±0.38	<0.0001	1.99	1.33±0.63	2.77±0.45	<0.0001	2.63
Lat. occipital lobe	0.81±0.33	0.91±0.29	0.38	0.31	1.35±0.35	2.32±0.38	<0.0001	2.66
Sup. temporal lobe	0.94±0.37	1.35±0.29	0.005	1.22	1.46±0.65	2.83±0.61	<0.0001	2.17
Inf. temporal lobe	0.96±0.16	1.81±0.58	<0.0001	2.00	1.52±0.62	2.89±0.51	<0.0001	2.42
Hippocampus	0.78±0.18	0.97±0.18	0.008	1.01	1.53±0.31	1.82±0.32	0.08	0.93
Insula	0.85±0.16	1.09±0.22	0.007	1.30	1.54±0.48	2.35±0.38	<0.0001	1.87
Striatum	0.39±0.16	0.46±0.25	0.65	0.33	1.79±0.76	2.98±0.64	0.0004	1.71
Subcortical white matter[a]	1.61±0.12	1.90±0.17	0.002	2.01	2.14±0.28	2.41±0.37	0.10	0.83
Neocortical	0.82±0.10	1.13±0.07	<0.0001	3.42	1.46±0.61	2.88±0.48	<0.0001	2.59

All images were partial volume corrected and then scaled and sampled. All results are adjusted for age
HC healthy control, *AD* Alzheimer's disease, *THK* ^{18}F-THK523, *PIB* ^{11}C-Pittsburgh compound B, *SUVR* standardized uptake value ratio, *d* Cohen's effect size *d*
[a] White matter SUVR are not partial volume corrected

THK523 SUVR correlated strongly with THK523 DVR in all cortical regions with a correlation coefficient of r=0.85 (p<0.0001) for the mean global measure.

Regional analysis of the non-partial volume-corrected images revealed significantly higher cortical THK523 retention in AD (Supplementary Fig. 2a) than in HC and SD patients. THK523 retention was also significantly higher in subcortical white matter in AD (Table 2). The spillover from the high retention in white matter was likely to contribute substantially to the radioactivity measured in grey matter; therefore, PVC of the images, correcting for *both* cortical grey matter atrophy and for white matter spillover, was performed. The PVC SUVR derived from the summed 60–90 min were subsequently used to assess THK523 retention as well as comparison with PIB and for correlation with brain volumetrics and cognitive parameters (Table 2). After PVC, while little or no THK523 retention was observed in cortical areas in HC, THK523 retention in AD patients was most prominent in cortical association areas, where only the temporal, parietal, hippocampal, orbitofrontal, and posterior cingulate regions (Supplementary Fig. 2b), brain areas known from post-mortem studies to contain substantial amounts of tau deposits in AD [10, 11], remained significant (Table 2). No significant differences were observed between HC and SD patients using either THK523 (Supplementary Table 1) or PIB (Supplementary Table 2). Global THK523 PVC SUVR in HC was 0.82±0.10 compared to 1.13±0.07 in AD (p<0.0001, Cohen's d=3.4) (Fig. 2).

◀ **Fig. 2** Global and regional retention of ^{18}F-THK523 and ^{11}C-PIB in AD. **a** Box plots for ^{18}F-THK523 (*left top panel*) and ^{11}C-PIB (*right top panel*) showing the global SUVR of both tracers. **b** When cognitively unimpaired HC with high (*HC+*) or low (*HC–*) ^{11}C-PIB retention were examined separately, it was observed that while ^{18}F-THK523 retention in isocortex of individuals with high ^{11}C-PIB retention aligned with those with low ^{11}C-PIB retention ^{18}F-THK523 retention in hippocampus and insula were not significantly different from the ^{18}F-THK523 retention in AD. *Red dotted lines* denote the bottom quartile of THK523 SUVR in AD patients. **c** Average parametric ^{18}F-THK523 transaxial and coronal partial volume-corrected (*PVC*) PET images overlaid on MRI of ten HC and ten AD patients, showing higher hippocampal and insular ^{18}F-THK523 retention on three HC with high (*HC+*) ^{11}C-PIB retention compared with seven HC with low (*HC–*) ^{11}C-PIB retention

Comparison of THK523 and PIB cortical retention

While seven of the ten HC and the three SD patients showed low Aβ burdens, all the AD patients and three HC presented with high Aβ burdens in the brain. In AD patients, the topographical pattern of cortical THK523 retention was clearly different from the cortical retention observed with PIB. While PIB was highest in the frontal, posterior cingulate, striatum and temporal cortices, THK523 was highest in temporal, parietal, hippocampus and posterior cingulate (Supplementary Fig. 3a). There was no correlation between the cortical THK523 SUVR and cortical PIB SUVR in the AD patients (r=0.04, p=0.90) (Supplementary Fig. 3b). Interestingly, in those HC with high Aβ burden (PIB+HC) while cortical THK523 retention was not significantly different to the cortical retention in PIB− HC, THK523 retention in the

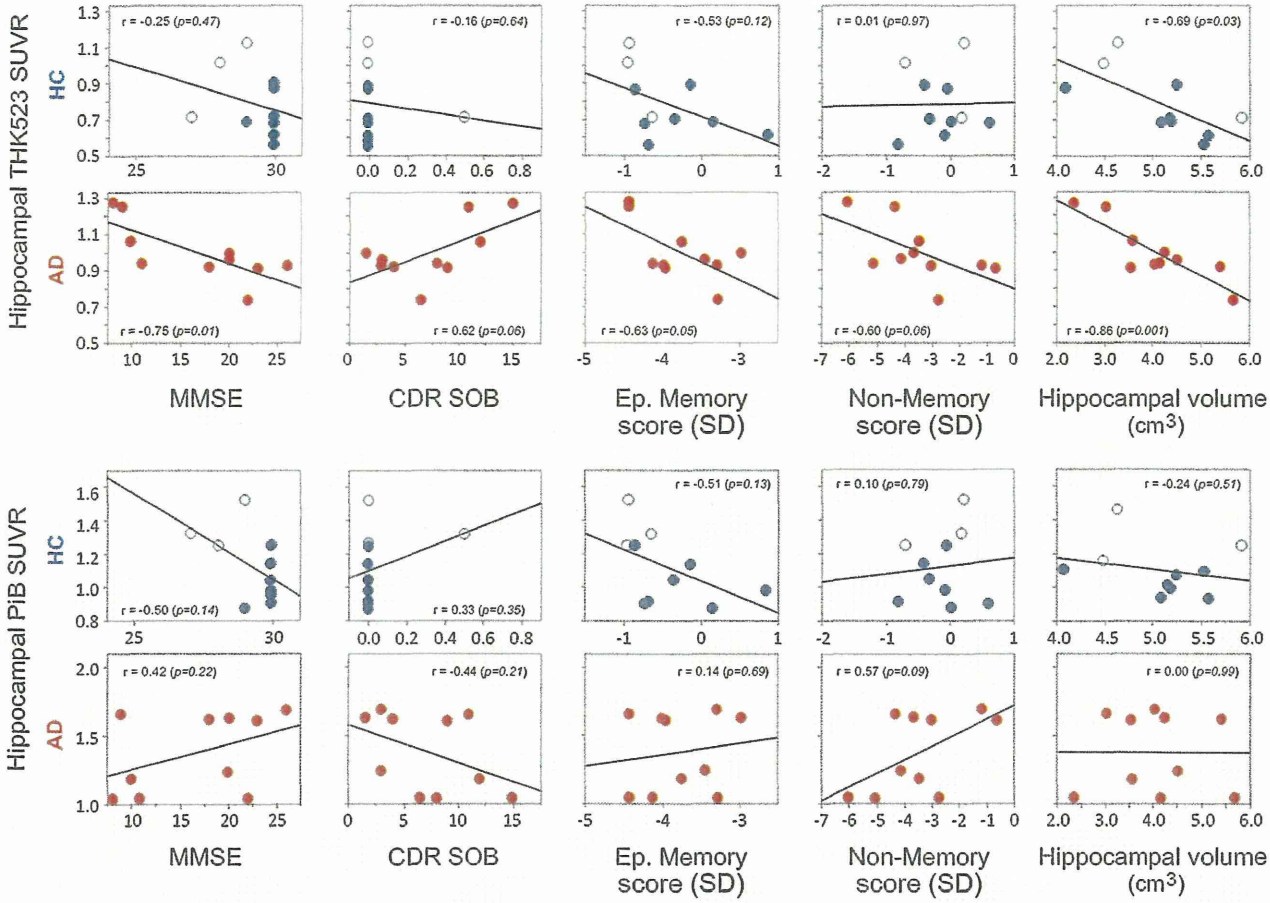

Fig. 3 Relationship between hippocampal ^{18}F-THK523 and ^{11}C-PIB retention with cognition and hippocampal volume. Regression analysis shows that while hippocampal ^{18}F-THK523 retention is not associated with cognition in HC, it is strongly associated with different cognitive parameters in AD patients (*top two rows*). On the other hand, hippocampal ^{18}F-THK523 retention is strongly associated with hippocampal volume in both HC and AD patients. There was no association between hippocampal ^{11}C-PIB retention (*bottom two rows*) with either cognitive parameters or hippocampal volume in any of the groups examined. All correlations were adjusted for age

hippocampus and insula was significantly higher than PIB− HC, but not significantly different from AD (Fig. 2).

Association between THK523 retention, cognition and brain volumetrics

While providing evidence of the general direction of the association between the different parameters (e.g. higher tau burden, lower cognitive performance), the associations derived from assessing all groups together tend to yield spurious correlations driven by the significant differences between the clinical groups. In order to avoid this issue, the associations with cognition and brain volumetrics were assessed in each clinical group separately.

In the case of THK523, there were no associations between cortical THK523 retention and cognitive parameters in HC, with the exception of the insula associated with episodic memory scores (r=−0.70, p=0.026). In the AD group, hippocampal THK523 retention was significantly associated with MMSE (r=−0.75, p=0.01) and episodic memory (r=−0.63, p=0.05) (Fig. 3). In the AD group, a strong trend was also observed between hippocampal THK523 retention, CDR SOB (r=0.62, p=0.055) and non-memory scores (r=−0.60, p=0.056). In regard to brain volumes, only hippocampal THK523 retention was significantly associated with hippocampal volume in both the HC (r=−0.69, p=0.03) and AD (r=−0.86, p=0.001) groups (Fig. 3). There were no correlations between global THK523 retention and cortical grey matter volume in any of the groups.

In the case of PIB, there were associations between PIB retention and MMSE in the orbitofrontal (r=−0.67, p=0.034), anterior (r=−0.65, p=0.04) and posterior cingulate (r=−0.78, p=0.007) regions of HC. In AD, there were some associations between PIB retention and cognitive parameters, but these correlations were, in every case, in the opposite direction as expected, where PIB retention in the anterior cingulate gyrus was positively associated with MMSE (r=0.63, p=0.049),

episodic memory (r=0.73, p=0.016) and non-memory scores (r=0.64, p=0.046) and inversely associated with CDR SOB (r=−0.68, p=0.03). There were no associations between hippocampal PIB retention and any cognitive parameter in any of the clinical groups (Fig. 3). There were no significant associations between global PIB retention and cortical grey matter volume in either HC or AD patients. In contrast to what was observed for hippocampal THK523 retention, there was no association between hippocampal PIB retention and hippocampal volume in any of the groups examined (Fig. 3).

Discussion

To the best of our knowledge, this is the first time a selective tau imaging agent has been thoroughly evaluated in human volunteers, assessing its associations with cognition and brain volumetrics, as well as a direct comparison with Aβ imaging using PIB.

Global cortical THK523 binding provided a very robust separation of AD patients from healthy elderly subjects (Cohen's d=3.4). Furthermore, cortical THK523 retention in AD patients followed the reported histopathological brain distribution of PHF-tau in AD [10, 11]. Examination of the brain kinetics of THK523 showed that it presents reversible binding kinetics, reaching apparent steady state about 50 min after injection of the radiotracer. Visual inspection of the THK523 images was hampered by the very high retention in white matter. In addition to the high non-specific binding, previous reports have demonstrated substantial concentrations of PHF-tau in white matter in AD [34, 35], suggesting THK523 retention in white matter might not solely reflect marked non-specific binding, but also some small degree of specific binding. Several factors were taken into account for the selection of the reference region. To date, no report has described tau deposition in the cerebellar cortex in sporadic AD [36]. There were no group differences in cerebellar cortex THK523 SUV, and there was no association between cerebellar cortex THK523 SUV with age in the whole cohort, or with dementia severity in the AD group, further supporting the use of the cerebellar cortex as reference region.

The regional brain distribution of THK523 showed a marked contrast when compared to that of PIB. While the highest PIB retention was observed in frontal, posterior cingulate, caudate and temporal cortices, the highest THK523 retention was observed in the inferior temporal, orbitofrontal, hippocampus, insula and parietal cortices. This was further confirmed by a lack of correlation between PIB SUVR and THK523 SUVR (r=0.04, p=0.90).

SD patients were included in the evaluation of THK523 as pathological controls [31]. Rather than tau aggregates, the vast majority of SD cases have been associated with the aggregation of TDP-43 [2, 31]. SD patients showed neither THK523 nor PIB retention in the brain (Supplementary Tables 1 and 2), suggesting the absence of both Aβ [37] and tau deposits in SD.

Three HC showed high cortical PIB retention (PIB+HC), consistent with previous PIB studies that have reported positive scans in 25–35 % of normal elderly individuals [38]. Despite the limited subsample size the finding is interesting because while cortical THK523 retention in PIB+HC was not significantly different from the cortical retention in PIB− HC, THK523 retention in the hippocampus and insula was significantly higher than in PIB− HC, but not significantly different from AD, suggesting that tau deposition in these regions might precede the dementia of AD [6, 39]. These findings might indicate that the combination of widespread cortical Aβ plus hippocampal tau deposition might not be enough to lead to significant cognitive impairment, requiring tau deposition in polymodal and unimodal association areas of the brain for objective cognitive impairment to be manifest [7, 10, 11].

As with Aβ imaging [40], longitudinal studies will assist in establishing the spatiotemporal patterns of tau deposition and help determine whether or not apparently healthy individuals with substantial hippocampal tau deposition will develop the AD phenotype, thus allowing very early, even preclinical diagnosis of AD, or if hippocampal tau deposits are just an age-associated process and only cortical tau deposition leads to cognitive impairment [39, 41].

In AD, hippocampal THK523 retention was associated with cognitive parameters. Similarly, hippocampal THK523 retention was associated with hippocampal volume in both HC and AD patients. Human post-mortem studies have shown that the density of NFTs strongly correlates with neurodegeneration and cognitive deficits, while Aβ plaque density does not [42, 43], a finding that was further confirmed through Aβ imaging studies [18, 32]. Furthermore, in stark contrast with Aβ plaques, NFTs are usually not present in associating cortical regions in cognitively unimpaired individuals [11, 18, 39].

As was previously reported in vitro [21, 44], several lines of evidence support the notion that THK523 selectively binds to PHF-tau and not to Aβ in vivo: (a) cortical THK523 retention is significantly higher in AD, following the known distribution of PHF-tau in the AD brain; (b) PIB and THK523 show different brain regional distribution patterns; (c) there is no correlation between PIB and THK523 retention; and (d) while hippocampal THK523 retention significantly correlates with cognitive parameters and hippocampal atrophy, hippocampal PIB retention does not.

While this was a first-in-human study, the limited sample size requires cautious interpretation of the findings. Furthermore, while our results suggest that ^{18}F-THK523 can reliably quantify PHF-tau deposition in vivo, there are serious limitations associated with the tracer itself. The high white matter THK523 retention, even if it might reflect some small degree of specific binding, precludes simple visual inspection of the

images and requires additional careful PVC even for a simple semi-quantitative analysis, preventing the use of THK523 in research or clinical settings.

Conclusion

This study has shown that despite selective, non-invasive in vivo assessment of PHF-tau in humans being possible, a single aspect of the in vivo behaviour of a tracer can derail its further development. This highlights the need for careful in vivo proof of concept studies at the initial stages of the development before embarking on more complex quantification approaches involving invasive procedures such as arterial cannulation or engaging in costly phase II studies. Better tau tracers, some of them already being evaluated in humans [23, 25–27], will be required for applications such as monitoring disease progression and assessing efficacy of anti-tau therapy. The development of ^{18}F-THK523 has shown to be a significant step towards the integration of tau imaging with Aβ imaging, moving us towards meeting the desired goal of earlier diagnosis of AD to assist the development of preventative treatments as well as identifying subjects for early therapeutic interventions.

Acknowledgements We thank Prof. Michael Woodward, Dr. John Merory, Dr. Gordon Chan, Dr. Kenneth Young, Dr. David Darby, Ms. Fiona Lamb and the Brain Research Institute for their assistance with this study. The study was partially supported by an Alzheimer Drug Discovery Foundation Research Grant (20101208 AFTD) and by a National Health and Medical Research Council of Australia Project Grant 1044361. The funding sources had no input into the design and conduct of the study; collection, management, analysis and interpretation of the data; and in the preparation, review, approval or decision to submit the manuscript for publication.

Conflicts of interest None.

References

1. Masters CL, Cappai R, Barnham KJ, Villemagne VL. Molecular mechanisms for Alzheimer's disease: implications for neuroimaging and therapeutics. J Neurochem 2006;97(6):1700–25. doi:10.1111/j.1471-4159.2006.03989.x.
2. Rabinovici GD, Miller BL. Frontotemporal lobar degeneration: epidemiology, pathophysiology, diagnosis and management. CNS Drugs 2010;24(5):375–98. doi:10.2165/11533100-000000000-00000.
3. Mohorko N, Bresjanac M. Tau protein and human tauopathies: an overview. Zdrav Vestn 2008;77(Suppl II):35–41.
4. Komori T. Tau-positive glial inclusions in progressive supranuclear palsy, corticobasal degeneration and Pick's disease. Brain Pathol 1999;9(4):663–79.
5. McKee AC, Cantu RC, Nowinski CJ, Hedley-Whyte ET, Gavett BE, Budson AE, et al. Chronic traumatic encephalopathy in athletes: progressive tauopathy after repetitive head injury. J Neuropathol Exp Neurol 2009;68(7):709–35. doi:10.1097/NEN.0b013e3181a9d503.
6. Delacourte A. Tauopathies: recent insights into old diseases. Folia Neuropathol 2005;43(4):244–57.
7. Buée L, Bussière T, Buée-Scherrer V, Delacourte A, Hof PR. Tau protein isoforms, phosphorylation and role in neurodegenerative disorders. Brain Res Brain Res Rev 2000;33(1):95–130.
8. Mandelkow E, von Bergen M, Biernat J, Mandelkow EM. Structural principles of tau and the paired helical filaments of Alzheimer's disease. Brain Pathol 2007;17(1):83–90. doi:10.1111/j.1750-3639.2007.00053.x.
9. Braak H, Braak E. Evolution of neuronal changes in the course of Alzheimer's disease. J Neural Transm Suppl 1998;53:127–40.
10. Braak H, Braak E. Staging of Alzheimer's disease-related neurofibrillary changes. Neurobiol Aging 1995;16(3):271–8. discussion 278–84.
11. Delacourte A, David JP, Sergeant N, Buée L, Wattez A, Vermersch P, et al. The biochemical pathway of neurofibrillary degeneration in aging and Alzheimer's disease. Neurology 1999;52(6):1158–65.
12. Goedert M, Jakes R. Mutations causing neurodegenerative tauopathies. Biochim Biophys Acta 2005;1739(2–3):240–50.
13. Roberson ED, Scearce-Levie K, Palop JJ, Yan F, Cheng IH, Wu T, et al. Reducing endogenous tau ameliorates amyloid beta-induced deficits in an Alzheimer's disease mouse model. Science 2007;316(5825):750–4.
14. Wischik CM, Edwards PC, Lai RY, Roth M, Harrington CR. Selective inhibition of Alzheimer disease-like tau aggregation by phenothiazines. Proc Natl Acad Sci U S A 1996;93(20):11213–8.
15. Brunden KR, Zhang B, Carroll J, Yao Y, Potuzak JS, Hogan AM, et al. Epothilone D improves microtubule density, axonal integrity, and cognition in a transgenic mouse model of tauopathy. J Neurosci 2010;30(41):13861–6. doi:10.1523/JNEUROSCI.3059-10.2010.
16. Bulic B, Pickhardt M, Mandelkow EM, Mandelkow E. Tau protein and tau aggregation inhibitors. Neuropharmacology 2010;59(4–5):276–89. doi:10.1016/j.neuropharm.2010.01.016.
17. Villemagne VL, Furumoto S, Fodero-Tavoletti MT, Harada R, Mulligan RS, Kudo T, et al. The challenges of tau imaging. Future Neurol 2012;7(4):409–21.
18. Rowe CC, Ng S, Ackermann U, Gong SJ, Pike K, Savage G, et al. Imaging beta-amyloid burden in aging and dementia. Neurology 2007;68(20):1718–25. doi:10.1212/01.wnl.0000261919.22630.ea.
19. Small GW, Kepe V, Ercoli LM, Siddarth P, Bookheimer SY, Miller KJ, et al. PET of brain amyloid and tau in mild cognitive impairment. N Engl J Med 2006;355(25):2652–63.
20. Okamura N, Suemoto T, Furumoto S, Suzuki M, Shimadzu H, Akatsu H, et al. Quinoline and benzimidazole derivatives: candidate probes for in vivo imaging of tau pathology in Alzheimer's disease. J Neurosci 2005;25(47):10857–62.
21. Fodero-Tavoletti MT, Okamura N, Furumoto S, Mulligan RS, Connor AR, McLean CA, et al. 18F-THK523: a novel in vivo tau imaging ligand for Alzheimer's disease. Brain 2011;134(Pt 4):1089–100. doi:10.1093/brain/awr038.
22. Zhang W, Arteaga J, Cashion DK, Chen G, Gangadharmath U, Gomez LF, et al. A highly selective and specific PET tracer for imaging of tau pathologies. J Alzheimers Dis 2012;31(3):601–12. doi:10.3233/JAD-2012-120712.
23. Chien DT, Bahri S, Szardenings AK, Walsh JC, Mu F, Su MY, et al. Early clinical PET imaging results with the novel PHF-tau radioligand [F-18]-T807. J Alzheimers Dis 2013;34(2):457–68. doi:10.3233/JAD-122059.
24. Shao XM, Carpenter GM, Desmond TJ, Sherman P, Quesada CA, Fawaz M, et al. Evaluation of [11C]N-methyl lansoprazole as a radiopharmaceutical for PET imaging of tau neurofibrillary tangles. ACS Med Chem Lett 2012;3(11):936–41.
25. Okamura N, Furumoto S, Harada R, Tago T, Yoshikawa T, Fodero-Tavoletti M, et al. Novel 18F-labeled arylquinoline derivatives for noninvasive imaging of tau pathology in Alzheimer disease. J Nucl Med 2013;54(8):1420–7. doi:10.2967/jnumed.112.117341.

26. Maruyama M, Shimada H, Suhara T, Shinotoh H, Ji B, Maeda J, et al. Imaging of tau pathology in a tauopathy mouse model and in Alzheimer patients compared to normal controls. Neuron 2013;79(6):1094–108. doi:10.1016/j.neuron.2013.07.037.
27. Chien DT, Szardenings AK, Bahri S, Walsh JC, Mu F, Xia C, et al. Early clinical PET imaging results with the novel PHF-tau radioligand [F18]-T808. J Alzheimers Dis 2014;38:171–84. doi:10.3233/JAD-130098.
28. Pike VW. PET radiotracers: crossing the blood–brain barrier and surviving metabolism. Trends Pharmacol Sci 2009;30(8):431–40. doi:10.1016/j.tips.2009.05.005.
29. McKhann G, Drachman D, Folstein M, Katzman R, Price D, Stadlan EM. Clinical diagnosis of Alzheimer's disease: report of the NINCDS-ADRDA Work Group under the auspices of Department of Health and Human Services Task Force on Alzheimer's Disease. Neurology 1984;34:939–44.
30. McKhann GM, Albert MS, Grossman M, Miller B, Dickson D, Trojanowski JQ, et al. Clinical and pathological diagnosis of frontotemporal dementia: report of the Work Group on Frontotemporal Dementia and Pick's Disease. Arch Neurol 2001;58(11):1803–9.
31. Hodges JR, Patterson K. Semantic dementia: a unique clinicopathological syndrome. Lancet Neurol 2007;6(11):1004–14.
32. Villemagne VL, Pike KE, Chételat G, Ellis KA, Mulligan RS, Bourgeat P, et al. Longitudinal assessment of Aβ and cognition in aging and Alzheimer disease. Ann Neurol 2011;69(1):181–92. doi:10.1002/ana.22248.
33. Price JC, Klunk WE, Lopresti BJ, Lu X, Hoge JA, Ziolko SK, et al. Kinetic modeling of amyloid binding in humans using PET imaging and Pittsburgh Compound-B. J Cereb Blood Flow Metab 2005;25(11):1528–47.
34. Mukaetova-Ladinska EB, Harrington CR, Roth M, Wischik CM. Biochemical and anatomical redistribution of tau protein in Alzheimer's disease. Am J Pathol 1993;143(2):565–78.
35. Khatoon S, Grundke-Iqbal I, Iqbal K. Levels of normal and abnormally phosphorylated tau in different cellular and regional compartments of Alzheimer disease and control brains. FEBS Lett 1994;351(1):80–4.
36. Larner AJ. The cerebellum in Alzheimer's disease. Dement Geriatr Cogn Disord 1997;8(4):203–9.
37. Rabinovici GD, Jagust WJ, Furst AJ, Ogar JM, Racine CA, Mormino EC, et al. Abeta amyloid and glucose metabolism in three variants of primary progressive aphasia. Ann Neurol 2008;64(4):388–401.
38. Rowe CC, Ellis KA, Rimajova M, Bourgeat P, Pike KE, Jones G, et al. Amyloid imaging results from the Australian Imaging, Biomarkers and Lifestyle (AIBL) study of aging. Neurobiol Aging 2010;31(8):1275–83. doi:10.1016/j.neurobiolaging.2010.04.007.
39. Delacourte A, Sergeant N, Wattez A, Maurage CA, Lebert F, Pasquier F, et al. Tau aggregation in the hippocampal formation: an ageing or a pathological process? Exp Gerontol 2002;37(10–11):1291–6.
40. Villemagne VL, Burnham S, Bourgeat P, Brown B, Ellis KA, Salvado O, et al. Amyloid beta deposition, neurodegeneration, and cognitive decline in sporadic Alzheimer's disease: a prospective cohort study. Lancet Neurol 2013;12(4):357–67. doi:10.1016/S1474-4422(13)70044-9.
41. Price JL, Morris JC. Tangles and plaques in nondemented aging and "preclinical" Alzheimer's disease. Ann Neurol 1999;45(3):358–68.
42. Arriagada PV, Growdon JH, Hedley-Whyte ET, Hyman BT. Neurofibrillary tangles but not senile plaques parallel duration and severity of Alzheimer's disease. Neurology 1992;42(3 Pt 1):631–9.
43. McLean CA, Cherny RA, Fraser FW, Fuller SJ, Smith MJ, Beyreuther K, et al. Soluble pool of Abeta amyloid as a determinant of severity of neurodegeneration in Alzheimer's disease. Ann Neurol 1999;46(6):860–6.
44. Harada R, Okamura N, Furumoto S, Tago T, Maruyama M, Higuchi M, et al. Comparison of the binding characteristics of [18F]THK-523 and other amyloid imaging tracers to Alzheimer's disease pathology. Eur J Nucl Med Mol Imaging 2013;40(1):125–32. doi:10.1007/s00259-012-2261-2.

Authors' contributions

Dr. Villemagne had full access to all the data in the study and takes responsibility for the integrity of the data and the accuracy of the data analysis

Drs. Villemagne, Furumoto, Fodero-Tavoletti, Kudo, Rowe and Okamura participated in the design, acquisition, analysis and interpretation of the data and writing of this manuscript.

Study concept and design: Villemagne, Okamura, Kudo, Rowe

Acquisition of data: Villemagne, Rowe, Fodero-Tavoletti, Pejoska, Yates, Piguet, Mulligan

Analysis and interpretation of data: Villemagne, Doré, Rowe, Okamura

Drafting of the manuscript: Villemagne, Okamura

Critical revision of the manuscript for important intellectual content: Villemagne, Furumoto, Rowe, Harada, Fodero-Tavoletti, Piguet, Hodges, Yanai, Masters, Kudo, Okamura

Statistical analysis: Villemagne, Okamura

Study supervision: Villemagne, Okamura

Curr Neurol Neurosci Rep (2014) 14:500
DOI 10.1007/s11910-014-0500-6

NEUROIMAGING (DJ BROOKS, SECTION EDITOR)

Tau PET Imaging in Alzheimer's Disease

Nobuyuki Okamura · Ryuichi Harada · Shozo Furumoto · Hiroyuki Arai · Kazuhiko Yanai · Yukitsuka Kudo

Published online: 21 September 2014

Abstract In several neurodegenerative diseases that are collectively called tauopathies, progressive accumulation of tau in the brain is closely associated with neurodegeneration and cognitive impairment. Noninvasive detection of tau protein deposits in the brain would be useful to diagnose tauopathies as well as to track and predict disease progression. Recently, several tau PET tracers including T807, THK-5117, and PBB3 have been developed and succeeded in imaging neurofibrillary pathology in vivo. For use of tau PET as a biomarker of tau pathology in Alzheimer's disease, PET tracers should have high affinity to PHF-tau and high selectivity for tau over amyloid-β and other protein deposits. PET tau imaging enables the longitudinal assessment of the spatial pattern of tau deposition and its relation to amyloid-β pathology and neurodegeneration. This technology could also be applied to the pharmacological assessment of anti-tau therapy, thereby allowing preventive interventions.

Keywords Positron emission tomography · Amyloid · Tau · Neurofibrillary tangles · Dementia · Early diagnosis · Biomarker

This article is part of the Topical Collection on *Neuroimaging*

N. Okamura · K. Yanai
Department of Pharmacology, Tohoku University School of Medicine, 2-1, Seiryo-machi, Aoba-ku, Sendai 9808575, Japan

K. Yanai
e-mail: yanai@med.tohoku.ac.jp

N. Okamura (✉) · R. Harada · Y. Kudo
Division of Neuro-imaging, Institute of Development, Aging and Cancer, Tohoku University, 4-1, Seiryo-machi, Aoba-ku, Sendai 9808575, Japan
e-mail: nookamura@med.tohoku.ac.jp

R. Harada
e-mail: dragon1@med.tohoku.ac.jp

Y. Kudo
e-mail: kudoyk3y7k3@med.tohoku.ac.jp

S. Furumoto
Frontier Research Institute for Interdisciplinary Science, Tohoku University, 6-3, Aoba, Aramaki, Aoba-ku, Sendai 9808578, Japan
e-mail: furumoto@cyric.tohoku.ac.jp

S. Furumoto
Cyclotron and Radioisotope Center, Tohoku University, 6-3, Aoba, Aramaki, Aoba-ku, Sendai 9808578, Japan

H. Arai
Department of Geriatrics and Gerontology, Institute of Development, Aging and Cancer, Tohoku University, 4-1, Seiryo-machi, Aoba-ku, Sendai 9808575, Japan
e-mail: harai@idac.tohoku.ac.jp

Introduction

Senile plaques (SPs) and neurofibrillary tangles (NFTs) are neuropathological hallmarks of Alzheimer's disease (AD). These protein deposits, SP and NFT, are composed of amyloid-β (Aβ) protein and hyperphosphorylated tau protein, respectively. A definitive diagnosis of AD can be established by the post mortem examination of the human brain. The amyloid cascade hypothesis, which proposes that abnormal production and accumulation of Aβ is the cause of AD, has been widely accepted as the concept of AD pathogenesis [1]. Preclinical amyloid pathology that has been observed in recent amyloid PET studies is considered as a high risk for future cognitive decline [2]. Many candidates for anti-amyloid drugs have been developed to reduce the amount of Aβ [3]. However, repeated failures of clinical trials for these drugs have increased, and shifted, our interest in using tau as another target for novel drug development [4, 5].

Hyperphosphorylation of the tau protein in AD forms insoluble fibers named paired helical filaments (PHFs) [6, 7]. PHFs accumulate in the neuronal cytoplasm and form NFTs [8, 9]. Initially, NFTs occur in the transentorhinal area, followed by the involvement of the entorhinal cortex and hippocampus, progressing to the temporal cortex and the other cortical areas [10, 11]. Postmortem studies have shown that the NFT, but not the SP, load correlates with the severity of dementia and neurodegeneration [12, 13], suggesting a more direct effect of tau aggregation on neurodegeneration than Aβ.

To facilitate the development of anti-tau drugs, it is important to measure the pathologic time course of NFT formation in the human brain. Recent developments allow us to visualize NFTs in the human brain using positron emission tomography (PET) by measuring the distribution of intravenously administered radiotracers that selectively bind to NFTs. Also, PET imaging is potentially useful for monitoring treatment outcomes and selecting patients for anti-dementia therapy [14].

Requirement for Tau PET Tracers

For using PET as a biomarker of tau pathology, the imaging measures should be quantitative, reproducible, and directly linked to the presence of tau deposits in the brain. Recently, several PET tracers have been developed for imaging tau pathology in the human brain [15–17]. Most of these tracers bind to the β-pleated sheet structure of tau protein fibrils in the same way as amyloid PET ligands. Therefore, these tracers are considered to be insensitive to tau oligomers. The ideal characteristics of tau-selective PET tracers are listed in Table 1. For successful imaging of NFTs in the AD brain, the tracer should have high binding affinity to PHF-tau. The binding affinity of tracers can be quantitatively evaluated by protein-ligand binding assay using synthetic tau fibrils or human brain homogenates. The assay using synthetic protein fibrils is widely used for the screening of protein-binding ligands. However, the measured value from synthetic fibrils should be interpreted cautiously because these fibrils do not completely imitate the conformation of native tau deposits.

The assay using human brain samples is a more reliable method for the assessment of protein-ligand interaction than using synthetic fibrils. This method has been used for the assessment of amyloid-binding PET ligands [18, 19]. Most amyloid PET ligands exhibit high binding affinities to AD brain homogenates (Kd or Ki<20 nM) [20–23]. Tau PET ligands are also required to exhibit similar affinity to AD brain samples in region where NFTs are frequent (e.g. entorhinal cortex, hippocampus, and temporal cortex). In AD neocortex, the concentrations of tau are ~5–20 times lower than those of Aβ [16]. Therefore, tracers should be highly selective for tau over Aβ. Simulation studies estimate that a 20-50-fold selectivity for PHF-tau over Aβ will be required for selective imaging of PHF-tau in vivo [24]. The most reliable method for the assessment of radioligand binding selectivity is autoradiography of human brain sections, because the binding of ligands to tau fibrils can be directly assessed at a low nanomolar ligand concentration, which is achieved in the brain tissue during a PET scan. If the ligand has autofluorescence, ligand binding can also be evaluated microscopically. However, this method generally requires micromolar concentration of ligands, which is far higher than radiotracer concentrations in the brain. Lipophilic fluoro-amyloid β-sheet binding PET tracers tend to accumulate in the white matter as well as Alzheimer cortex, possibly because myelin contains β-sheet structures. Such non-specific white matter tracer binding needs to be kept minimal when developing PET ligands for tau.

In addition to these binding properties, radiotracers should have high blood–brain barrier (BBB) permeability. Most successful amyloid-PET tracers show an initial brain uptake above 4 % of the injected dose (%ID) at 2 min after intravenous injection in mice [23, 25, 26]. Lipophilicity is one of the most important determinants of BBB permeability. Ideally, a radiotracer should exhibit LogP values between 0.9 and 2.5 [27]. In addition, radiotracers should be cleared rapidly from background and non-target areas. Slower clearance of radiotracers prolongs the time for them to reach a secular equilibrium in a PET study. The brain 2-to-30 min ratio in normal mice is a good index of the clearance of radiotracer from non-target areas. The

Table 1 Ideal characteristics of tau PET tracers

Characteristics	Requirements
High binding affinity for PHF-tau	Kd or Ki<20 nM for tau-rich brain samples
High binding selectivity for PHF-tau	>20 fold selectivity for PHF-tau over Aβ
High blood–brain barrier permeability	>4 % ID/g at 2 min post injection in normal mice
Rapid clearance from normal brain tissue	2 min-to-30 min brain uptake ratio in mice>10
Moderate lipophilicity	LogP=1–3
Low non-specific binding	Low or no binding to subcortical white matter
Low metabolism	Metabolites should not enter into the brain

successful amyloid PET tracer [^{11}C]PiB shows high 2-to-30 min ratio (>10), reflecting a fast clearance from non-target regions [23]. An ideal radiotracer should readily enter the brain and selectively bind to its target in the absence of radiolabeled metabolites. Thus, the radiolabeled metabolites should not penetrate BBB. ^{18}F-labeled tracers are more clinically useful than ^{11}C-labeled tracers as the longer lived ^{18}F isotope allows time for tracer delivery to many PET centers [28]. Three ^{18}F-labeled amyloid PET tracers, including [^{18}F]florbetapir (Amyvid™), [^{18}F]flutemetamol (Vizamyl™), [^{18}F]florbetaben (Neuraceq™), have become commercially available in EU and US. However, in some ^{18}F-labeled ligands, defluorination can cause bone accumulation of ^{18}F, which might interfere with visual assessment of tracer distribution in the brain.

Tau PET in Clinical Studies

FDDNP

The first successful PET tau imaging in humans was accomplished by using [^{18}F]FDDNP [29]. In the autoradiography of the AD brain sections raised [^{18}F]FDDNP binding was detected in the hippocampus where a high density of NFTs were observed by immunohistochemistry [30]. Patients with AD and 50 % of mild cognitive impairment (MCI) cases showed higher [^{18}F]FDDNP retention than healthy control subjects [31]. A direct comparison between FDDNP and PiB in the same AD patients found negligible PiB but strong FDDNP binding in the medial temporal cortex, compatible with FDDNP binding to NFTs [32]. However, FDDNP uptake was also increased in amyloid rich cortical association areas in AD. Intriguingly, recent [^{18}F]FDDNP PET study demonstrated an elevated FDDNP uptake in the subcortical brain areas and amygdala of football players suspected of chronic traumatic encephalopathy (CTE) [33], suggesting the potential utility of PET imaging for monitoring pathological tau deposits after traumatic brain injury [34]. Furthermore, [^{18}F]FDDNP is reported to be sensitive in imaging the regional localization of tau deposits in progressive supranuclear palsy (PSP) [35]. However, there are some limitations for use of this tracer as a biomarker of tau, because this tracer binds non-selectively to both SPs and NFTs and is less sensitive to tau deposits than more recently developed radiotracers shown below.

PBB3

[^{11}C]PBB3 is a PET tracer that is reported to allow in vivo detection of tau deposits in AD as well as in non-AD tauopathies, including PSP and corticobasal degeneration (CBD) [36•]. In clinical PET studies, this tracer can be produced with sufficient radioactivity and high quality [37] and it clearly differentiated AD brains from healthy control brains [36•]. [^{11}C]PBB3 retention in the hippocampus of AD patients confirms the binding ability of this tracer to NFTs. In addition, this study reported significant [^{11}C]PBB3 binding to tau deposits in the basal ganglia of a CBD case. Ongoing multicenter PET studies of [^{11}C]PBB3 will validate the clinical usefulness of this tracer in various types of tauopathies.

T807 and T808

[^{18}F]T807 and [^{18}F]T808 have been developed as tau-selective PET tracers [38•, 39, 40]. In vitro autoradiography studies showed that both radiotracers exhibit strong and selective binding to PHF-tau with nanomolar affinity on AD brain sections with little binding to amyloid plaques. The first-in-man PET study successfully demonstrated [^{18}F]T807 retention in the frequent areas of PHF-tau in the AD brain [38•]. In addition, [^{18}F]T807 retention was associated with increased disease severity. There was much more elevated and extensive [^{18}F]T807 retention in severe AD case than in MCI and mild AD cases. Unlike most ^{18}F-labeled amyloid PET tracers, [^{18}F]T807 shows very low non-specific binding of the tracer to the white matter, which may improve the grey-to-white matter contrast in the brain. The first-in-man PET studies of [^{18}F]T808 were performed in 11 subjects [39]. This tracer showed more rapid tracer distribution throughout the brain and more rapid clearance from normal brain tissue than [^{18}F]T807. Most AD cases showed elevated [^{18}F]T808 retention in the frequent areas of PHF-tau. However, substantial defluorination was observed in some cases.

THK-523, THK-5105 and THK-5117

Novel quinoline derivatives were initially identified as candidates for tau PET tracer by the screening of over 2,000 small molecules [41]. In vitro autoradiography studies using three ^{18}F-labeled derivatives ([^{18}F]THK-523, [^{18}F]THK-5105 and [^{18}F]THK-5117) demonstrated the high binding selectivity of these tracers to tau over Aβ on AD brain sections [42–44]. While [^{18}F]THK-523 PET failed to clearly visualize tau deposits in the human brain in vivo [45],. [^{18}F]THK-5105 PET successfully demonstrated radiotracer retention in sites susceptible to tau deposition in the AD brain [46••]. Recent [^{18}F]THK-5117 PET studies demonstrated higher signal-to-background ratio and better pharmacokinetics of this tracer than [^{18}F]THK-5105 [17]. [^{18}F]THK-5117 PET images in mild, moderate and severe AD patients are shown in Fig. 1. These tracer retentions were associated with clinical severity of dementia and brain atrophy [46••], which is consistent with the observation of postmortem brain analysis showing the association of tau pathology with dementia severity and neuronal loss.